Proceedings of the
Annual Stability Conference
Structural Stability Research Council
San Antonio, Texas, March 21-24, 2017

Spherically-Hinged Short-to-Intermediate Angle Columns: Stability, Non-Linear Behavior and DSM Design

Pedro B. Dinis[1], Dinar Camotim[1]

Abstract

This work reports a numerical investigation on the buckling, post-buckling (elastic and elastic-plastic), strength and design of spherically-hinged short-to-intermediate equal-leg angle columns. It extends the scope of similar studies recently carried out by the authors for cold-formed and hot-rolled (lower leg width-to-thickness ratios) steel fixed and pin-ended angles with the same characteristics. After briefly reviewing the most relevant findings unveiled in the above studies, the paper addresses the buckling behavior of spherically-hinged columns – the results presented and discussed, which include the selection of the column geometries to be considered, are obtained by means of Generalized Beam Theory (GBT). Then, the post-buckling behavior and strength of columns containing initial geometrical imperfections and residual stresses (special attention is paid to modeling the latter in hot-rolled angles) is investigated. The results obtained, by means of ABAQUS shell finite element analyses, include a parametric study intended to gather failure load data covering a wide slenderness range. The above numerical failure loads are subsequently used to develop, validate and assess the merits of a rational design approach for such members, which is based on the Direct Strength Method (DSM) and adopts ideas and procedures similar to those employed recently by the authors (Dinis & Camotim 2015, 2016a,b, Dinis *et al.* 2016) in the context of fixed-ended and pin-ended (cylindrical hinges) short-to-intermediate equal-leg angle columns. The need for modifications arises from the change in major-axis flexure support conditions, which influences the column flexural-torsional behavior significantly. It is shown that the proposed/modified DSM strength curves lead to safe and reliable failure load predictions for spherically-hinged short-to-intermediate equal-leg angle columns exhibiting a wide slenderness range, thus extending the scope of the existing rational DSM-based design approach to cover also columns with these end support conditions.

1. Introduction

A few years ago, Dinis *et al.* (2012) investigated the mechanical behaviors of cold-formed steel fixed and pin-ended short-to-intermediate equal-leg angle columns. In particular, they unveiled that such mechanical behaviors are (i) both strongly influenced by the interaction between flexural-torsional and flexural buckling (a unique global-global interaction) and (ii) markedly different, due to effective centroid shift effects appearing in the pin-ended columns. The above findings led Dinis & Camotim (2015) to propose a novel, rational and unified design approach applicable to both fixed and pin-ended columns, which is based on the Direct Strength Method (DSM – *e.g.*, Schafer 2008, Camotim *et al.* 2016) and combines

[1] CERIS, ICIST, DECivil, Instituto Superior Técnico, Universidade de Lisboa, Portugal. <dinis; dcamotim@civil.ist.utl.pt>

(i) numerically-based genuine flexural-torsional strength/design curves, specifically developed for this purpose, with (ii) the currently codified DSM global design curve. This design approach was shown to be both accurate and reliable – indeed, the prediction quality of the available experimental and numerical failure loads allows for the use of an LRFD resistance factor equal ϕ_c=0.85, value recommended for all compression members by the current North American Specification (AISI 2016). The above design approach was subsequently slightly improved by Landesmann *et al.* (2016) and, finally cast in a simpler form, better suited for codification, by Dinis & Camotim (2016b).

Quite recently, Dinis *et al.* (2016) and Dinis & Camotim (2016a) extended the research activity described in the previous paragraph and investigated, numerically, the behavior and DSM-based design of hot-rolled steel fixed and pin-ended short-to-intermediate equal-leg angle columns, which differ from their cold-formed counterparts in the fact that they (i) exhibit much stockier legs (lower width-to-thickness ratios) and (ii) are visibly affected by residual stress effects. These numerical studies provided fairly solid evidence that the DSM-based design approach developed for cold-formed steel columns can also be readily applied to hot-rolled ones counterparts – experimental results are needed in order to confirm these findings (they are planned for the not too distant future).

However, all the work on pin-ended columns carried out so far concerned end supports (i) pinned with respect to minor-axis flexure and (ii) fixed with respect to major-axis flexure and torsion – support conditions corresponding to rigid plates resting on cylindrical hinges that are often considered in experimental investigations (*e.g.*, Popovic *et al.* 1999, Landesmann *et al.* 2016) and will be termed here "PC columns". The aim of this paper is to present the results of an ongoing numerical investigation dealing with the stability, non-linear behavior and DSM design of a different type of pin-ended short-to-intermediate equal-leg angle columns, namely those with end support conditions corresponding to rigid plates resting on spherical hinges: (i) pinned with respect to major and minor-axis flexure and (ii) fixed only with respect to torsion – such columns will be termed here "PS columns".

Following a brief overview of the most relevant findings of the investigations mentioned in the previous paragraph, recently reported for similar F (fixed-ended columns) and PC columns, the paper presents and discusses the results obtained from a study concerning the buckling behavior of PS columns with various leg slenderness values ($b/t \leq 20$ or $b/t > 20$), carried out by means of Generalized Beam Theory (GBT) and leading to the mechanical characterization of the columns analyzed in this work. Moreover, the buckling behaviors of F, PC and PS columns are compared, in order to unveil the differences between them. Then, the paper addresses the post-buckling (elastic and elastic-plastic) and failure behavior of PS columns. The results presented and discussed are obtained through ABAQUS shell finite element analyses (SFEA), including both initial geometrical imperfections and residual stresses (special attention is paid to modeling the latter in stocky-leg angles – $b/t \leq 20$), and comprising a parametric study aimed at gathering a representative set of failure load data that covers a wide slenderness range. These numerical failure loads, together with experimental test results collected from the literature (for hot-rolled angles), are subsequently employed to assess the quality of their estimates provided by the DSM-based design approach proposed by Dinis & Camotim (2015) for F and PC cold-formed steel columns (and later shown to be valid also for their hot-rolled counterparts – Dinis *et al.* 2016). It is shown that the above design approach needs to be modified before it can be successfully applied to PS columns – the modifications arise from the change in major-axis flexure support conditions, which influences the column flexural-torsional behavior significantly. Finally, the paper presents the development/proposal of new expressions for the DSM strength/design curves and provides solid evidence that the lead efficient (safe and reliable) failure load predictions for the short-to-intermediate PS columns considered in this

work, which exhibit a wide slenderness range, thus extending the scope of the existing rational DSM-based design approach to cover also columns with these (spherically-hinged) end support conditions.

2. Brief Review of the Behavior and Design of Hot-Rolled F and PC Columns

This section summarizes the main findings unveiled in recent investigations concerning the buckling, post-buckling and DSM design of F and PC short-to-intermediate angle columns with stocky legs (low width-to-thickness ratios), namely hot-rolled steel angle columns with $b/t \leq 20$ (Dinis *et al*. 2016, Dinis & Camotim 2016a). The curves in Figs. 1(a)-(b), obtained with GBTUL (Bebiano *et al*. 2008), show the variation of the critical stress f_{cr} with the length L (logarithmic scale) for F and PC columns with three leg widths (b=50; 70; 90 mm) and various wall thickness values, corresponding to b/t=7.5; 10; 15; 25. As for Figs. 2(a)-(b), they show the upper parts (P/P_{cr}>0.4) of the column equilibrium paths P/P_{cr} *vs.* β (β is the mid-span torsional rotation) for F and PC columns with (i) b/t=10; 15; 20; 58 (the last one illustrates the behavior of a typical cold-formed steel column) and (ii) L equal to $\approx 0.25\,L_{T.F}$ (Fig. 2(a_1)), $0.5\,L_{T.F}$ (Fig. 2(a_2)), $0.75\,L_{T.F}$ (Fig. 2(a_3)) and $L_{T.F}$ (Fig. 2(a_4)), or (iii) L equal to $\approx 0.25\,L_{T.PC}$ (Fig. 2(b_1)), $0.5\,L_{T.PC}$ (Fig. 2(b_2)), $0.75\,L_{T.PC}$ (Fig. 2(b_3)) and $L_{T.PC}$ (Fig. 2(b_4)), where $L_{T.F}$ and $L_{T.PC}$ are the column lengths corresponding to the transition between flexural-torsional and flexural buckling in F and PC columns, respectively. All the columns analyzed contain critical-mode initial imperfections with small amplitudes (10% of the wall thickness t). On the other hand, Figs. 3(a)-(b) plot the variation, with $L/L_{T.F}$ or $L_{T.PC}$, of the ratio χ, measuring the failure load drop caused by the residual stresses ($\chi=[(P_u - P_{u.rs})/P_u]\times 100$, where $P_{u.rs}$ and P_u are F and PC column failure loads with and without residual stresses).

Out of the various findings obtained from the aforementioned investigations, which led to the results displayed in Figs. 1 to 3, the following ones deserve to be specially mentioned:

(i) In F columns, (i_1) f_{cr} corresponds to single half-wave buckling and decreases monotonically with L, (i_2) torsion is highly predominant in the flexural-torsional buckling mode and (i_3) the critical buckling mode nature switches abruptly from (major-axis) flexural-torsional to (minor-axis) flexural at $L=L_{T.F}$. The flexural-torsional buckling stress f_{crft} is given by the formula (Dinis & Camotim 2015)

$$f_{bt} = G\frac{t^2}{b^2} + \pi^2 \frac{E\,t^2}{12\,(L/2)^2} \qquad f_{bf} = \pi^2 \frac{E\,b^2}{6\,(L/2)^2} \qquad f_{crft} = \frac{4}{5}\left(f_{bt} + f_{bf} - \sqrt{(f_{bt}+f_{bf})^2 - 2.5\,f_{bt}\,f_{bf}} \right), \quad (1)$$

where $G=E/[2\,(1+\nu)]$ is the shear modulus and f_{bt} and f_{bf} are the angle column pure torsional and major-axis flexural buckling stresses, respectively.

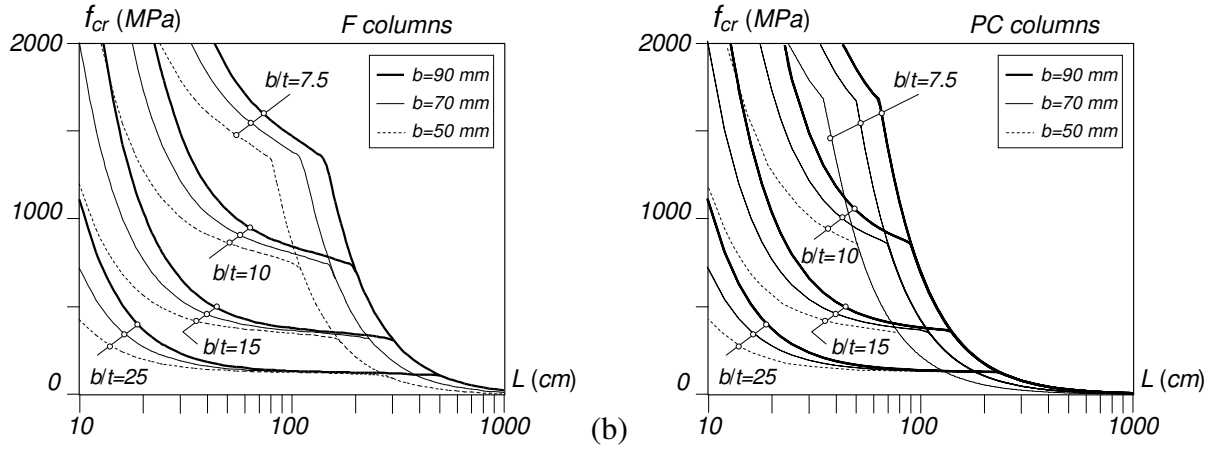

Figure 1: f_{cr} vs. L curves for (a) F and (b) PC columns with b=50; 70; 90 mm and leg slenderness values b/t=7.5; 10; 15; 25

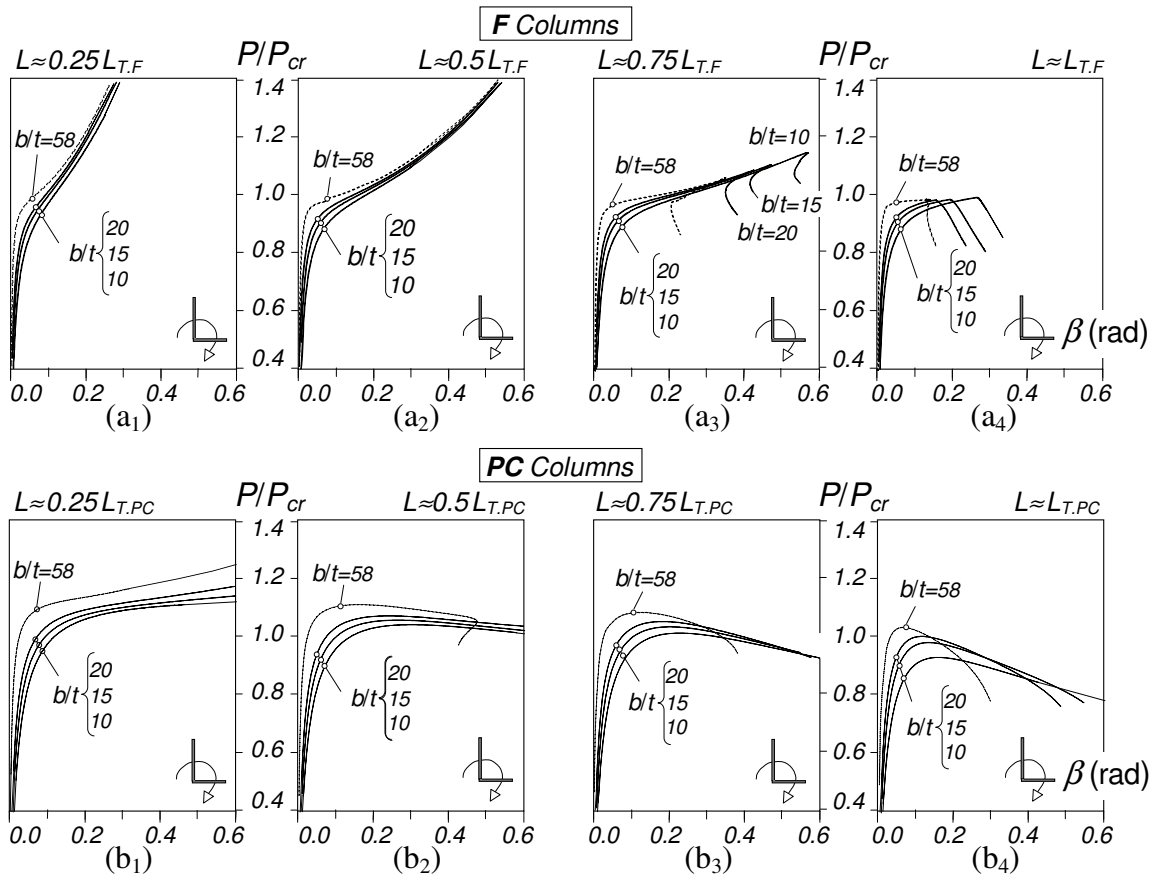

Figure 2: Angle columns with stocky legs: elastic equilibrium paths P/P_{cr} vs. β for (a) F and (b) PC columns with (1) $L/L_T \approx 0.25$, (2) $L/L_T \approx 0.5$, (3) $L/L_T \approx 0.75$, (4) $L/L_T \approx 1.0$

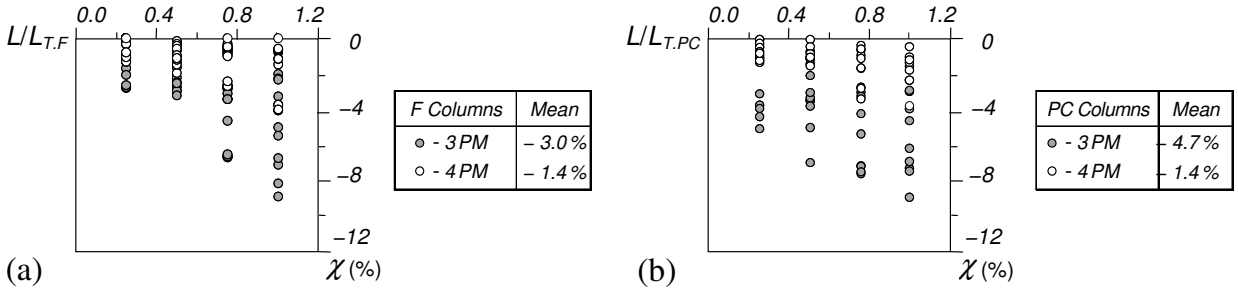

Figure 3: Hot-rolled steel angle columns: plots of (a) χ vs. $L/L_{T.F}$ (F columns) and (b) χ vs. $L/L_{T.PC}$ (PC columns)

(ii) Since the column minor-axis flexural buckling stress $f_{bf.m}=f_{bf}/4=\pi^2 E\, b^2/[24\times(L/2)^2$ is independent of t, the flexural-torsional (FT) buckling curves of all the F columns sharing the same leg width b end up in the same flexural buckling curve.

(iii) The critical stress $f_{cr.LT.F}$, corresponding to the simultaneous occurrence of flexural-torsional and flexural buckling (*i.e.*, concerning the F column with $L=L_{T.F}$) depends only on b/t and the steel material properties – naturally, the value of $L_{T.F}$ varies with b. The values of $f_{cr.LT.F}$ and $L_{T.F}$ can be calculated by means of the expressions

$$f_{cr.L_{T.F}} = \frac{E}{K_F} \qquad L_{T.F} = b\sqrt{\frac{\pi^2 K_F}{6}} \qquad \text{with} \quad K_F = (1+\nu)\left[2.25\left(\frac{b}{t}\right)^2 - 4.0\right] \quad . \quad (2)$$

(iv) Since the PC and F column buckling behaviors only differ in the length range associated with the "flexural-torsional plateau", the curves in Fig. 1(b) are identical to the F column ones (Fig. 1(a)) – *i.e.*, Eq. (1) also provides the PC columns flexural-torsional critical buckling stresses ($f_{cr.LT.PC}$). Now, due to the drop in minor-axis flexural buckling load ($f_{bf.m}=\pi^2 E\, b^2/[24\times L^2]$), the buckling mode nature switch (from flexural-torsional to flexural) occurs at $L_{T.F}=L_{T.PC}$. Moreover, the length of the "flexural-torsional plateau" decreases visibly with b/t – for $b/t<10$, such plateau does not even exist.

(v) In PC columns, the critical stress $f_{cr.LT.PC}$ (transition between FT and F buckling, at $L=L_{T.PC}$) and $L_{T.PC}$ values can be calculated by means of expressions identical to those in Eqs. (2), with the sole difference of the coefficient appearing in the expressions providing K_{PC} and K_F: 0.5125 vs. 2.25 (to account for the minor-axis flexural buckling load reduction). Thus, $f_{cr.LT.PC}$ and $L_{T.PC}$ (PC columns) are related to their F column counterparts ($f_{cr.LT.F}$ and $L_{T.F}$) by

$$f_{cr.L_{T.PC}} = \frac{0.5625\,(b/t)^2 - 1.0}{0.5125\,(b/t)^2 - 4.0}\; f_{cr.L_{T.F}} \qquad L_{T.PC} = \sqrt{\frac{0.5125\,(b/t)^2 - 4.0}{2.25\,(b/t)^2 - 4.0}}\; L_{T.F} \quad . \quad (3)$$

(vi) The hot-rolled and cold-formed steel columns, which differ considerably in leg slenderness, share key post-buckling behavioral features, namely the strong length-dependent interaction between (major-axis) flexural-torsional and (minor-axis) flexural buckling – *e.g.*, it is responsible for the occurrence of the elastic limit points in the equilibrium paths depicted in Figs. 2(a_3)-(a_4) (F columns). This interaction is much more severe in PC columns, as can be clearly observed in Figs. 2(b_2)-(b_4).

(vii) Finally, the hot-rolled F and PC column failure loads are not visibly lowered by the residual stresses. Indeed, their impact on the column failure load is not very significant: in average, the failure load drop is equal to 3% and 4.7%, respectively for F and PC columns – see Figs. 3(a)-(b)).

The numerical failure loads gathered by Dinis *et al*. (2016) and Dinis & Camotim (2016a) were used to assess the prediction quality of the DSM design approaches proposed by Dinis & Camotim (2015), in the context of cold-formed steel angle columns. Figs. 4(a)-(b) clearly show that this quality is quite high – indeed, the averages and standard deviations of the numerical-to-predicted ultimate strength ratios (f_u/f_{nfte}) are equal to 1.07/0.06 and 1.08/0.12, respectively for the F and PC hot-rolled steel columns.

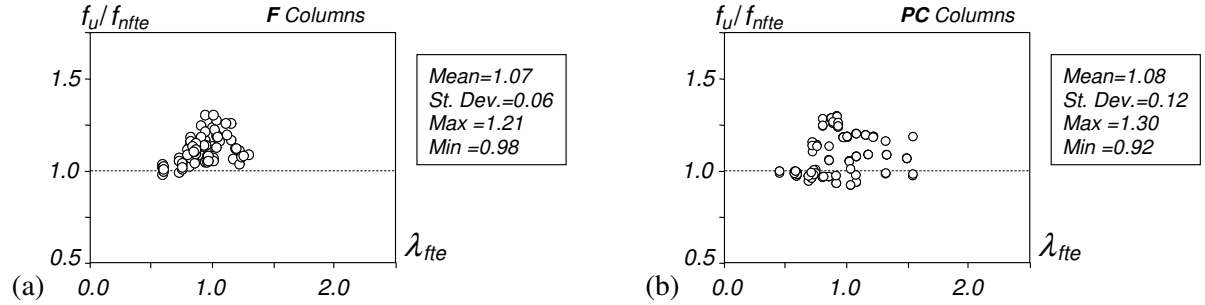

Figure 4: Plots of f_u/f_{nfte} vs. λ_{fte} for (a) F and (b) PC hot-rolled steel angle columns

3. PS Column Buckling Behavior

The f_{cr} vs. L (logarithmic scale) curves shown in Figs. 5(a)-(b), obtained through GBTUL buckling analyses, concern F, PC and PS columns with b=90 mm and b/t=20 (stocky legs – Fig. 5(a)) or b/t=40 (slender legs – Fig. 5(b)) – the GBT analyses included 7 deformation modes: 4 global (**1**-**4**) and 3 local (**5**-**7**). Finally, Fig. 5(c) shows 3 PS column buckling modes (L=25,100,500 cm) and 6 GBT deformation mode in-plane shapes (except axial extension). These buckling results prompt the following remarks:

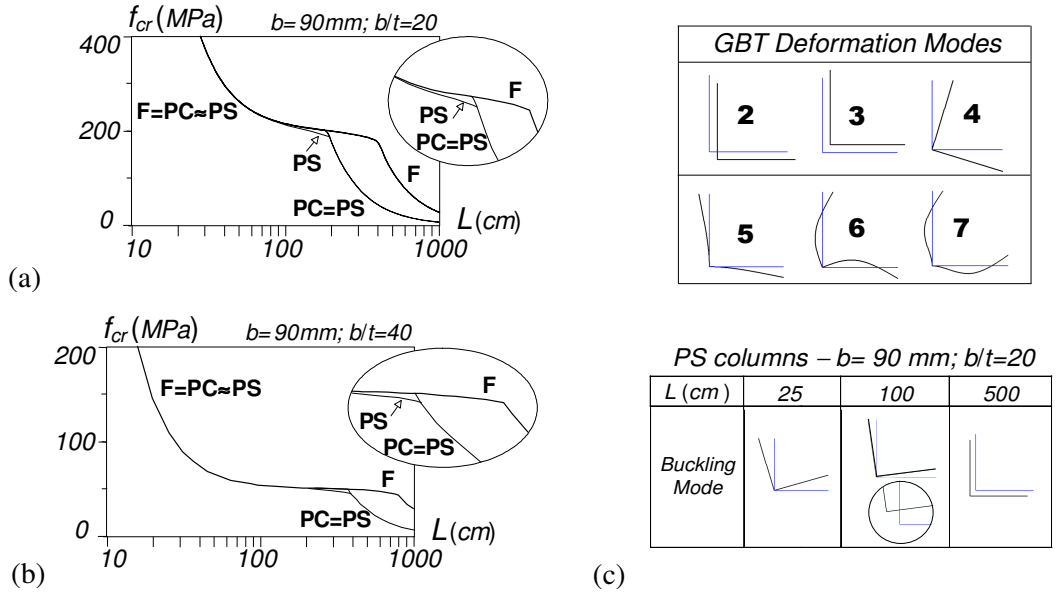

Figure 5: F, PC and PS columns (b=90mm): f_{cr} vs. L curves for (a) b/t=20 and (b) b/t=40 columns, (c) in-plane shapes of GBT deformations **2**-**7** and 3 PS column critical buckling modes (b/t=20)

(i) The buckling behaviors of the slender-leg (b/t=40) F and PC columns are identical to those reported by Dinis *et al*. (2012), in the context of cold-formed steel members. Indeed, (i_1) the mid portions of the f_{cr} vs. L curves consist of well defined "plateaus" associated with flexural-torsional (FT) buckling (the so-called "FT plateaus"), (i_2) the PC column behavior only differs from its F column counterpart in the length of the "FT buckling plateau" (due to the 75% drop of the minor-axis flexural buckling loads, the transition from FT buckling occurs for smaller lengths).

(ii) As for the PS column buckling behaviors, they differ from their PC column counterparts due to the change in major-axis flexure support conditions – naturally, the differences become more visible close to the transition to minor-axis flexural buckling. Indeed, the PS column FT buckling loads are slightly lower than the PC column and, therefore, the transition to minor-axis flexural (F) buckling occurs for a marginally higher length ($L_{T.PS}$=394cm vs. $L_{T.PC}$=376cm for b/t=40) – at $L_{T.PC}$, the PS column buckling load drop amounts to 7.6%, also for b/t= 40.

(iii) The main quantitative behavioral difference between stocky-leg (b/t=20) and slender-leg (b/t=40) columns concerns the "FT plateau": well defined in the latter and practically non-existent in the former (particularly in the PC and PS columns).

GBT provides further insight on the difference between the buckling behaviors of PC and PS columns with stocky and/or slender legs. Figs. 6(a)-(b) display the GBT modal participation diagrams, providing the contributions of each deformation mode (modes **1**-**7** shown in Fig. 5(c)) to the column critical buckling modes, corresponding to the f_{cr} vs. L curves shown in Figs. 5(a)-(b) – the tables quantify the amount of major-axis flexure (mode **2** – p_2) exhibited by the critical buckling modes of PC and PS columns with various short-to-intermediate lengths. These buckling results prompt the following remarks:

(i) In all the f_{cr} vs. L curve mid portions (associated with FT buckling), p_2 is initially minute and grows visibly as L increases – see the tables in Figs. 6(a)-(b), concerning columns with b/t=20 and b/t=40, respectively. Moreover, note that the p_2 value at the transition between FT and F buckling (L=$L_{T.PC}$ or L=$L_{T.PS}$) is practically the same for the columns with the two b/t values.

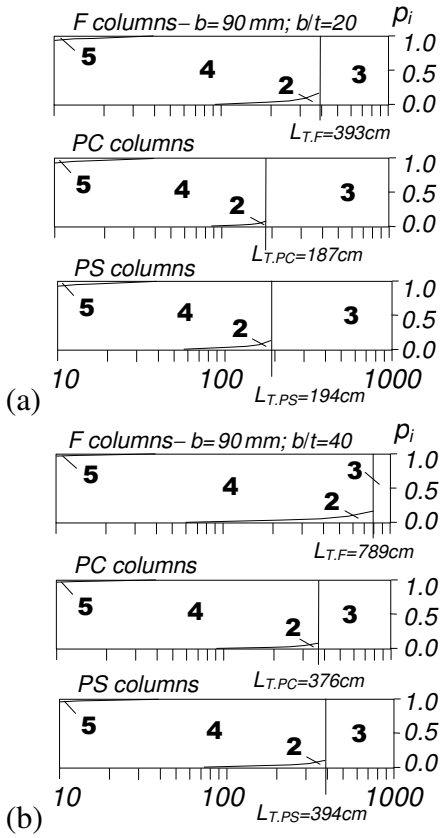

PC columns

L (cm)	p_2 (%)	Δ_f (%)
25	0.1	0.1
50	0.2	0.2
75	0.4	0.4
100	0.7	0.7
150	1.5	1.6
186($\approx L_{T.PC}$)	2.3	2.5

PS columns

L (cm)	p_2 (%)	Δ_f (%)
25	0.8	0.4
50	0.9	0.9
75	1.7	1.7
100	3.0	3.0
150	6.5	6.5
193($\approx L_{T.PS}$)	10.8	10.8

PC columns

L (cm)	p_2 (%)	Δ_f (%)
100	0.2	0.2
150	0.3	0.3
200	0.7	0.6
250	1.0	1.0
300	1.5	1.6
375($\approx L_{T.PC}$)	2.3	2.4

PS columns

L (cm)	p_2 (%)	Δ_f (%)
100	0.7	0.7
150	1.6	1.6
200	2.8	2.8
250	4.3	4.4
300	6.3	6.4
393($\approx L_{T.PS}$)	10.8	10.9

Figure 6: F, PC and PS columns (b=90 mm): GBT modal participation diagrams and critical buckling mode p_2 value for (a) b/t=20 and (b) b/t=40

(ii) Dinis & Camotim (2015) showed that there is a very good correlation between the variations, with L, of p_2 and the percentage drop of f_{crft} with respect to the pure torsional bucking stress f_{bt}, defined by $\Delta_f=[(f_{bt}-f_{crft})/f_{bt}]\times 100$ and whose values are also given in tables of Fig. 6(a)-(b). Note that p_2 and Δ_f are equal to 2.3%/2.5% and 10.8%/10.9%, respectively for slender and stocky-leg PC and PS columns with $L\approx L_{T.PC}$ and $L\approx L_{T.PS}$ – note that the latter values are similar to those reported by Dinis *et al*. (2016) for F columns with the much larger $L\approx L_{T.F}$ (p_2=10.2 and Δ_f=12.1). This increase in p_2 and Δ_f is bound to have significant impact on the design of PS equal-leg angle columns.

In order to investigate the influence of the leg slenderness on the PS column buckling behavior, Figs. 7(a) display 24 f_{cr} vs. L curves concerning columns with b=50, 70, 90 mm and two b/t ranges: $b/t\leq 20$ (7.5, 10, 15, 20 – Fig. 7(a_1)) and $b/t\geq 20$ (20, 25, 40, 58 – Fig. 7(a_2)) – note that Figs. 7(a_1) and 7(a_2) have different vertical scales and that the b/t=20 curves appear in both figures. Each curve was obtained by means of GBT buckling analyses including the aforementioned 7 deformation modes (see Fig. 5(c)). On the other hand, Figs. 7(b) display the GBT modal participation diagrams concerning the b=70 mm columns with b/t=7.5, 10, 15. Finally, Fig. 7(c) provides the variation of p_2 with L (normalized w.r.t $L_{T.PS}$). The observation of these buckling results leads to the following comments:

(i) The FT buckling curve portions concerning PC column trios sharing the same leg width b end up in the same F curve, since the column minor-axis flexural buckling stress ($f_{bf.m}=\pi^2 E b^2/[24\times L^2]$) does not depend on t. In addition, the critical stress $f_{cr.LT.PS}$, corresponding to the transition between FT and F buckling (at $L=L_{T.PS}$), only depends on b, b/t and the steel properties. The values of $f_{cr.LT.PS}$ and $L_{T.PS}$ can be calculated by means of expressions

$$f_{cr.L_{T.PS}} = \frac{E}{K_{PS}} \qquad L_{T.PS} = b\sqrt{\frac{\pi^2\, K_{PC}}{6}} \qquad \text{with} \quad K_{PS} = (1+\nu)\left[0.5625\left(\frac{b}{t}\right)^2 - 4.0\right] \quad . \quad (4)$$

Note that the above expressions are practically identical to those appearing in Eqs. (2) for F columns – the sole exception is the coefficient appearing in K_{PS}: 0.5625 instead of 2.25, to account for the minor-axis flexural buckling load reduction (in PC columns this coefficient is 0.5125). Therefore, the PS column critical stress $f_{cr.LT.PS}$ and transition length $L_{T.PS}$ are related to their F column counterparts ($f_{cr.LT.F}$ and $L_{T.F}$) by means of the expressions

$$f_{cr.L_{T.PS}} = \frac{2.25\,(b/t)^2 - 4.0}{0.5625\,(b/t)^2 - 4.0}\; f_{cr.L_{T.F}} \qquad L_{T.PS} = \sqrt{\frac{0.5625\,(b/t)^2 - 4.0}{2.25\,(b/t)^2 - 4.0}}\; L_{T.F} \quad . \quad (5)$$

(ii) The "FT plateau" length decreases visibly with b/t. Moreover, such "plateau" is well defined for column with slender legs (b/t>25) and virtually nonexistent for columns with stocky ones (b/t≤10).

(iii) The variation of p_2 (or Δ_f) with $L/L_{T.PS}$ is almost independent of b/t and b, particularly for L>0.5$L_{T.PS}$ (see Fig. 5(d)). In additions, the p_2 (or Δ_f) values of PS columns with L=$L_{T.PS}$ are significantly higher than those concerning PC columns with L≈$L_{T.PC}$ (see tables in Figs. 6(a)-(b)).

(iv) Finally, note the tiny contribution of the symmetric local mode **5** to the "flexural" buckling mode of PS columns with b/t<10 – this contribution (iv$_1$) has its maximum value for L=$L_{T.PS}$, (iv$_2$) grows as L increases and (iv$_3$) is higher for stockier legs (p_5 equals 0.07%, 0.04%, 0.01% for b/t =7.5, 10, 15).

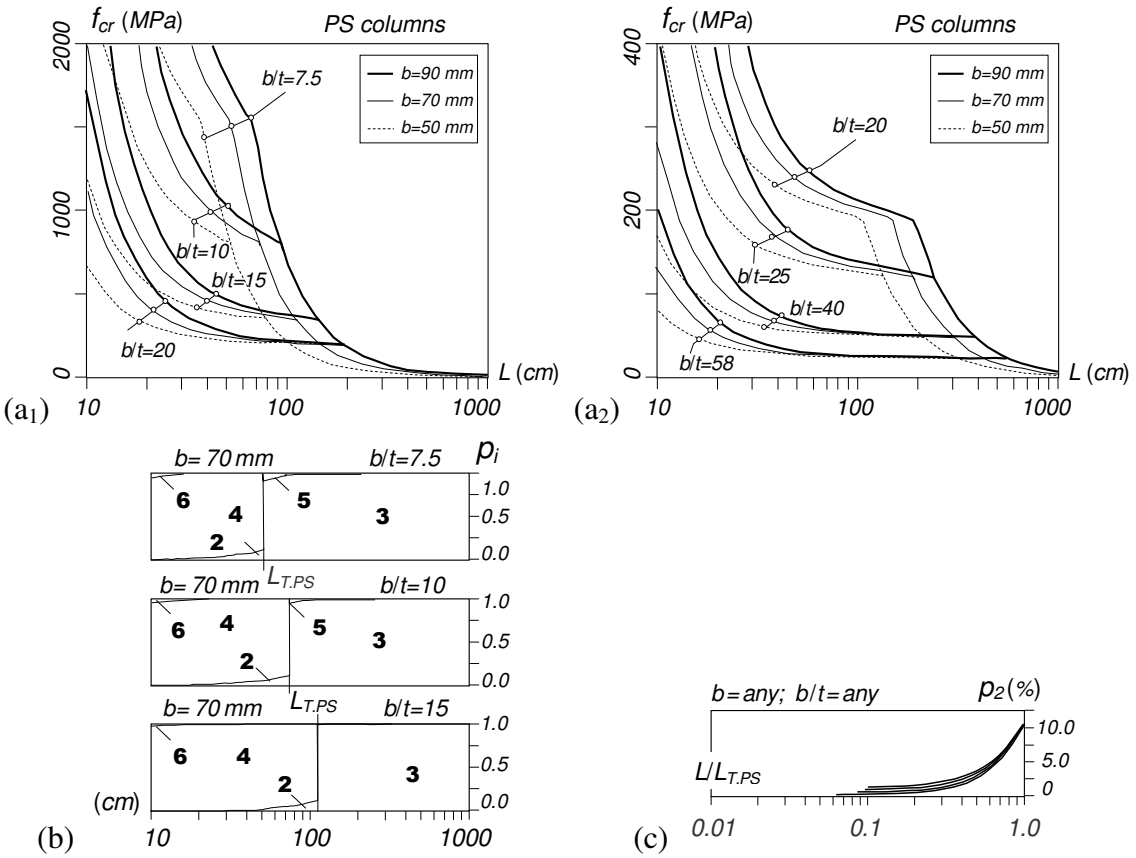

Figure 7: PS columns: (a) f_{cr} vs. L curves for (a$_1$) b/t≤20 and (a$_1$) b/t≥20, (b) GBT modal participation diagrams for b=70mm and b/t= 7.5, 10, 15, and (c) variation of p_2 with L (normalized w.r.t $L_{T.PS}$)

3.1 Column Geometry Selection

The geometries of short-to-intermediate columns with stocky legs ($b/t \leq 20$ – hot-rolled steel angles) were selected from the ArcelorMittal catalogue (2015), by enforcing (i) buckling in FT (predominantly torsional) modes and (ii) critical buckling stresses at $L=L_{T.PS}$ ($f_{cr.LT.PS}$) no higher than 700 MPa. Since the steel grades covered by the above catalogue have yield stresses not exceeding 450 MPa, the collapse of columns with critical stresses above this value is clearly governed by plasticity (stocky columns). Fig. 8(a) plots $f_{cr.LT.PS}$ against b/t for the whole set of cross-section dimensions covered by the ArcelorMittal catalogue and makes it possible to conclude that only 77 (out of 177) column geometries satisfy the enforced conditions – they correspond to the shaded area in Fig. 8(a), *i.e.*, are such that $b/t \geq 11$. Most of these column cross-section geometries lead to transition lengths $L_{T.PS}$ below 200 cm (as shown in Fig. 8(b), this applies to 47 of the 77 selected column geometries). The three column families analyzed in this work were chosen from the above selected 77 columns and their geometries (b, t, L, $L_{T.PS}$) are given in Table 1, together with the corresponding f_{cr} values. In order to enable assessing the relevance of the interaction between FT and F buckling, columns exhibiting four normalized lengths ($L \approx 1.0, 0.75, 0.5, 0.25\ L_{T.PS}$) are analyzed – the corresponding Δ_f values are also given in Table 1.

The geometries of short-to-intermediate columns with slender legs ($b/t > 20$ – cold-formed steel angles) were selected to have (i) b values as their stocky-leg counterparts, (ii) b/t=25,40,58, and (iii) 4 normalized lengths ($L \approx 1.0, 0.75, 0.5, 0.25\ L_{T.PS}$) – Table 2 shows these column geometries and f_{cr}-Δ_f values.

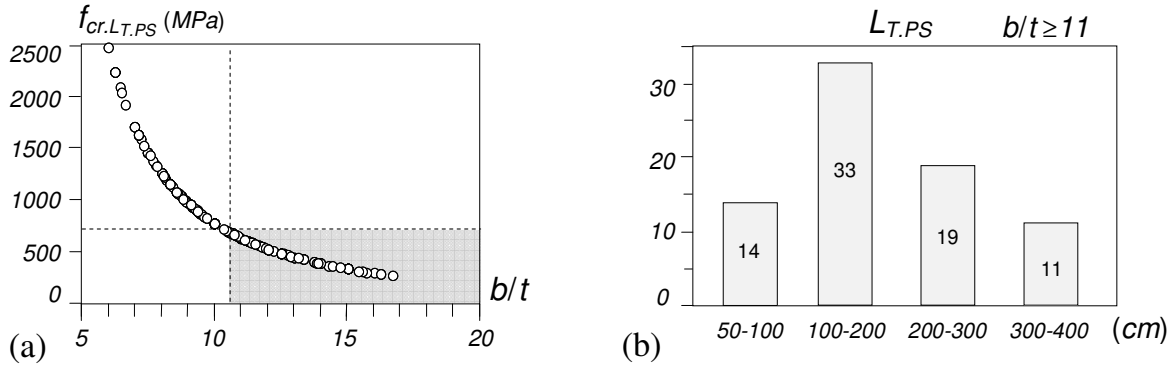

Figure 8: Hot-rolled angle column (($b/t \leq 20$)) selection: (a) $f_{cr.L_{T.P}}$ vs. b/t plot and (b) number of columns with $L_{T.PS}$ inside the indicated length intervals (such that $f_{cr.LT.PS} \leq 700$ MPa)

Table 1: Selected/analyzed angle column b, t, L, f_{cr} and Δ_f values (mm and MPa) – $b/t \leq 20$

b	t	b/t	$L \approx 0.25\ L_{T.PS}$ ($\Delta_f \approx 1.0$)		$L \approx 0.5\ L_{T.PS}$ ($\Delta_f \approx 3.0$)		$L \approx 0.75\ L_{T.PS}$ ($\Delta_f \approx 6.0$)		$L \approx L_{T.PS}$ ($\Delta_f \approx 11.0$)	
			L	f_{cr}	L	f_{cr}	L	f_{cr}	L	f_{cr}
50	4.55	11	146	1325.1	291	809.9	437	695.2	582	631.6
70	6.36		204	1324.8	408	809.8	611	695.1	815	631.6
90	8.18		263	1322.0	525	809.0	788	694.7	1050	631.1
50	3.33	15	202	542.7	403	394.4	605	356.3	806	329.9
70	4.67		283	542.2	565	394.2	848	356.1	1130	329.8
90	6		363	542.9	725	394.5	1088	356.3	1450	330.0
50	2.5	20	271	258.5	542	210.5	813	195.5	1080	183.1
70	3.5		379	258.8	565	210.6	1136	195.6	1514	183.0
90	4.5		488	258.6	975	210.6	1463	195.6	1950	183.0

Table 2: Selected/analyzed angle column b, t, L, f_{cr} and Δ_f values (mm and MPa) – $b/t>20$

b	t	b/t	$L\approx0.25\,L_{T.PS}$ ($\Delta_f\approx1.0$)		$L\approx0.5\,L_{T.PS}$ ($\Delta_f\approx3.0$)		$L\approx0.75\,L_{T.PS}$ ($\Delta_f\approx6.0$)		$L\approx L_{T.PS}$ ($\Delta_f\approx11.0$)	
			L	f_{cr}	L	f_{cr}	L	f_{cr}	L	f_{cr}
50	2	25	340	152.0	680	131.5	1020	123.8	1350	116.5
70	2.8		475	152.1	950	131.5	1425	123.8	1895	116.4
90	3.6		612	152.0	1224	131.5	1836	123.8	2440	116.4
50	1.25	40	545	53.7	1090	50.0	1635	47.8	2175	45.1
70	1.75		765	53.7	1529	50.0	2294	47.8	3045	45.1
90	2.25		983	53.7	1965	50.0	2948	47.8	3920	45.1
50	0.86	58	797	24.4	1594	23.3	2391	22.4	3183	21.2
70	1.2		1115	24.4	2230	23.3	3345	22.4	4455	21.2
90	1.54		1435	24.4	2870	23.3	4305	22.4	5735	21.2

4. PS Column Post-Buckling Behavior

4.1 Elastic Behavior

The elastic post-buckling behaviors of the selected 72 columns, all containing critical-mode initial geometrical imperfections with small amplitudes (10% of the wall thickness t), were determined by means of ABAQUS SFEA – all relevant modeling issues can be found in Dinis *et al*. (2007). Figs. 9(a)-(b) show the upper parts ($P/P_{cr}>0.4$) of the equilibrium paths P/P_{cr} *vs.* β (β is the mid-span torsional rotation) of columns with (i) $b/t\leq20$ (11, 15, 20 – Figs. 9(a_1)-(a_4)), (ii) $b/t\geq20$ (20, 25, 40, 58 – Figs. 9(b_1)-(b_4)), and(iii) lengths $L\approx0.25L_{T.PS}$, $0.5L_{T.PS}$, $0.75L_{T.PS}$ and $L_{T.PS}$ – note that the b/t=20 column paths appear in the two figures. The observation of these elastic post-buckling results prompts the following remarks:

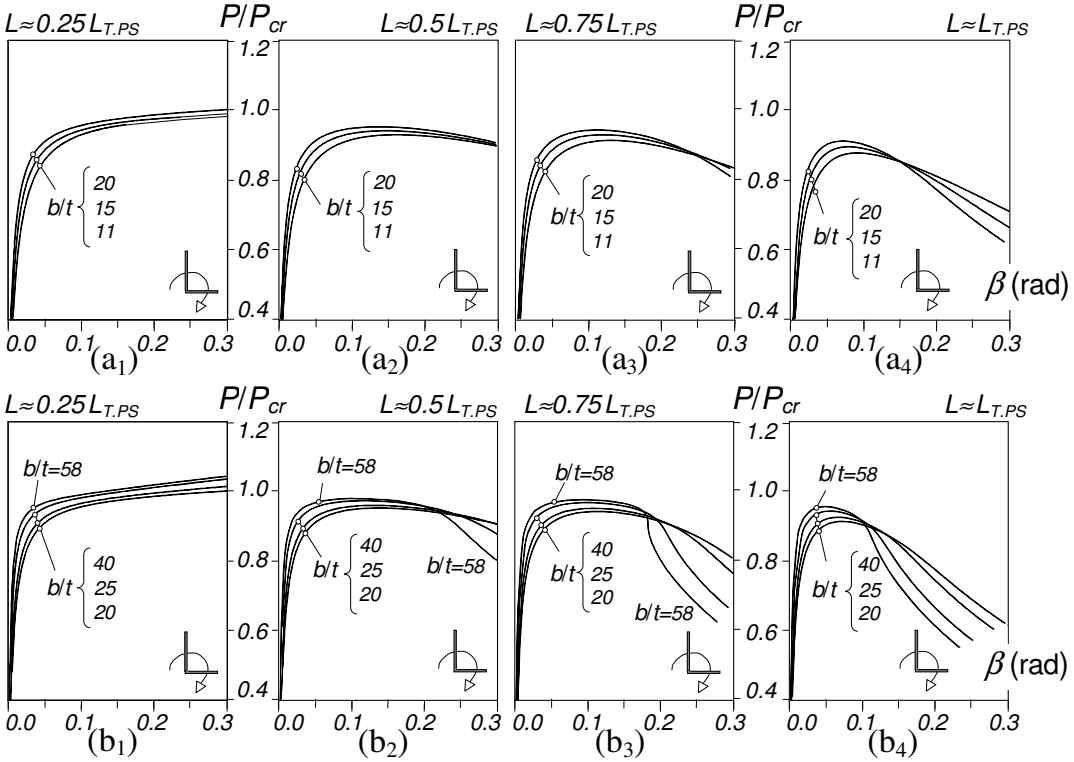

Figure 9: PS column elastic equilibrium paths P/P_{cr} *vs.* β for $L/L_{T.PS}\approx0.25$-1.0 and (a) $b/t\leq20$ or (b) $b/t\geq20$

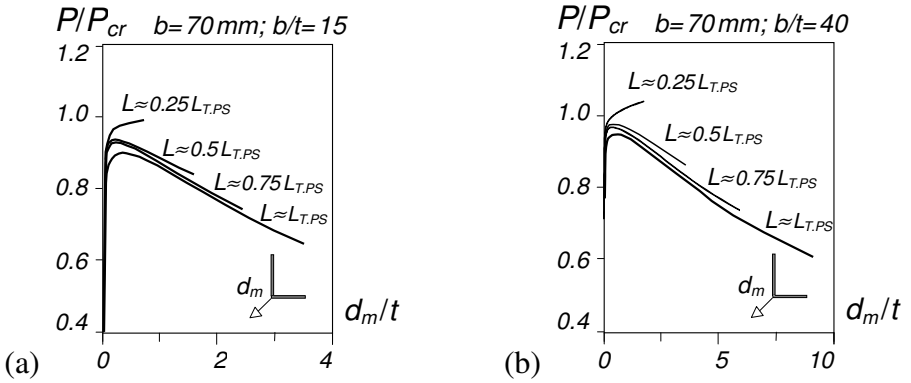

Figure 10: PS columns elastic equilibrium paths P/P_{cr} *vs.* d_m/t for $L/L_{T.PS}\approx$ 0.25-1.0 and (a) b/t=15 or (b) b/t=40

(i) Columns with identical b/t and $L/L_{T.PS}$ values exhibit practically coincident equilibrium paths, *i.e.*, post-buckling behaviors. Moreover, these post-buckling behaviors are almost independent of b/t – to confirm this assertion, compare the equilibrium paths in Figs. 9(a_1)-(a_2) with those in Figs. 9(b_1)-(b_2).

(ii) The post-buckling behaviors involve the simultaneous occurrence of cross-section torsional rotations and translations − the latter have a visible impact on the column post-buckling strength. As can be clearly observed in Figs. 9(a_3)-(a_4) and Figs. 9(b_3)-(b_4), two behavioral patterns can be identified: (ii_1) the one exhibited by the shortest columns ($L/L_{T.PS}\approx$0.25), corresponding to small translations and associated with the "expected" post-critical strength (but fairly small), and (ii_2) that exhibited by the remaining columns ($L/L_{T.PS}\approx$0.5–1.0), corresponding to significant translations and associated with well-defined limit points. It is worth noting that, in F columns, such limit points only occur for $L/L_{T.F}\geq$0.75 (see Fig. 2). In order to provide a better feel on the relevance of the cross-section translations, Figs. 10(a)-(b) display the equilibrium paths P/P_{cr} *vs.* d_m/t, where d_m is the mid-span translation due to minor-axis flexure, for the $L/L_{T.PS}\approx$0.25-1.0 columns with b=70 mm and either b/t=15 (Fig. 10(a)) or b/t=40 (Fig. 10(b)) − the qualitative difference between the $L/L_{T.PS}\approx$0.50-1.0 and $L/L_{T.PS}\approx$0.25 equilibrium paths is striking in both cases!

(iii) As the column length approaches $L_{T.PS}$, the limit points occur for smaller $P/P_{cr.PS}$ values − *e.g.*, the limit points of PS columns with b/t=15 occur at P_u/P_{cr}=0.94, 0.93, 0.90 for $L/L_{T.PS}\approx$0.50, 0.75, 1.00. These limit points are also slightly below their PC column counterparts, P_u/P_{cr}=0.95, 0.95, 0.93 (Dinis & Camotim 2016a − see Table 3).

Table 3: PS and PC columns $P/P_{cr.PS}$ values associated with elastic limit points

b/t	PS Columns			PC Columns (Dinis & Camotim 2016a)		
	$L/L_{T.PS}$			$L/L_{T.PC}$		
	0.5	0.75	1.0	0.5	0.75	1.0
11	0.93	0.91	0.88	0.95	0.93	0.91
15	0.94	0.93	0.90	0.95	0.95	0.93
20	0.95	0.94	0.91	0.96	0.96	0.95
25	0.96	0.95	0.92			
40	0.97	0.97	0.94			
58	0.98	0.98	0.96			

(iv) The above finding clearly shows that the PS columns are a slightly more prone to coupling between flexural-torsional and minor-axis flexural buckling than the PC columns, due to the lower flexural-torsional critical buckling loads. On the other hand, recall that, due to the absence of minor-axis end moments to oppose the bending caused by the effective centroid shift effects (Young & Rasmussen 1999), both columns share a high susceptibility to the above interaction phenomenon.

(v) Finally, concerning the post-buckling behavior, it is observed that a b/t decrease leads to (v_1) a bit more flexible equilibrium paths and (v_2) limit points taking place for slightly lower P/P_{cr} values and higher mid-span torsional rotations – *e.g.*, the $L/L_{T.PS} \approx 0.75$ exhibit $P_{max}=0.98\,P_{cr}$ at $\beta_{max}=0.09$, for $b/t=58$, and $P_{max}=0.91\,P_{cr}$ and $\beta_{max}=0.13$, for $b/t=11$.

4.2 Elastic-Plastic Behavior

Figs. 11(a)-(b) depict the upper portions ($P/P_{cr}>0.4$) of typical short column ($L\approx 0.25\,L_{T.PS}$) elastic-plastic equilibrium paths – they concern columns with $b=70$ mm, $b/t=15$ (Fig. 11(a)) or $b/t=40$ (Fig. 11(b)) and containing critical-mode initial imperfections with small amplitudes (10% of the wall thickness t): P/P_{cr} *vs.* β concerning yield-to-critical stress ratios $f_y/f_{cr}=1.0, 1.8, 2.5$ (the elastic equilibrium paths of Figs. 9(a_1)-(b_1) are also shown – they correspond to $f_y/f_{cr}=\infty$). Fig. 11(a) also displays three plastic strain diagrams, corresponding to equilibrium states located along the $f_y/f_{cr}\approx 1.8$ column equilibrium path and including the collapse mechanism. On the other hand, Figs. 12(a)-(b) show similar elastic-plastic results for typical intermediate-to-long ($L\approx 0.75\,L_{T.PS}$) columns with the same b and b/t values. The observation of all these results leads to the following remarks:

(i) Short columns with $f_y/f_{cr}>1.0$ exhibit very small elastic-plastic strength reserve and ductility prior to failure – *e.g.*, increasing the yield stress 2.5 times leads to a strength increase of about 20%, for columns with stocky legs, and about 10%, for columns with slender legs.

(ii) Diagram *I* in Fig. 11(a) shows that yielding starts at the end cross-section vicinity (vertical leg tip) and (ii_2) mid-span region (horizontal leg tip). Then, as displayed in Diagrams *II* and *III*, plasticity gradually evolves along both the column length and leg widths.

(iii) In the intermediate-to-long columns ($L\approx 0.75\,L_{T.PS}$), there is no benefit in having a yield stress much higher than f_{cr}, since the collapse will occur in the elastic range – see Figs. 12(a)-(b).

(iv) Diagram *I* in Fig. 12(a) shows that yielding only occurs well inside the equilibrium path descending branch – it starts at the ¼ and ¾-span cross-section vertical leg tips (where the longitudinal normal and shear stresses are higher – see Dinis *et al.* 2012) and precipitates failure.

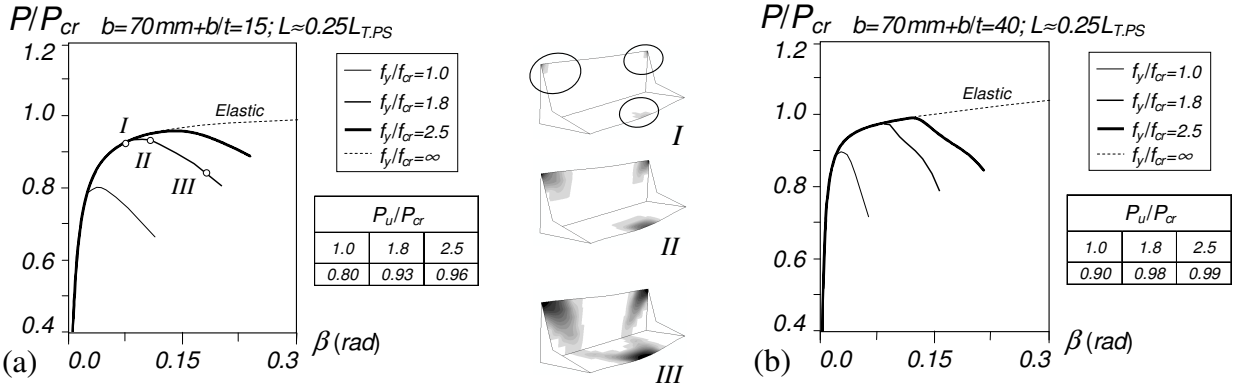

Figure 11: PS column elastic-plastic equilibrium paths P/P_{cr} *vs.* β for $L\approx 0.25\,L_{T.PS}$, $f_y/f_{cr}=1.0, 1.8, 2.5, \infty$ and (a) $b/t=15$ (plastic strain diagram evolution for the $f_y/f_{cr}\approx 1.8$ column also included) or (b) $b/t=40$

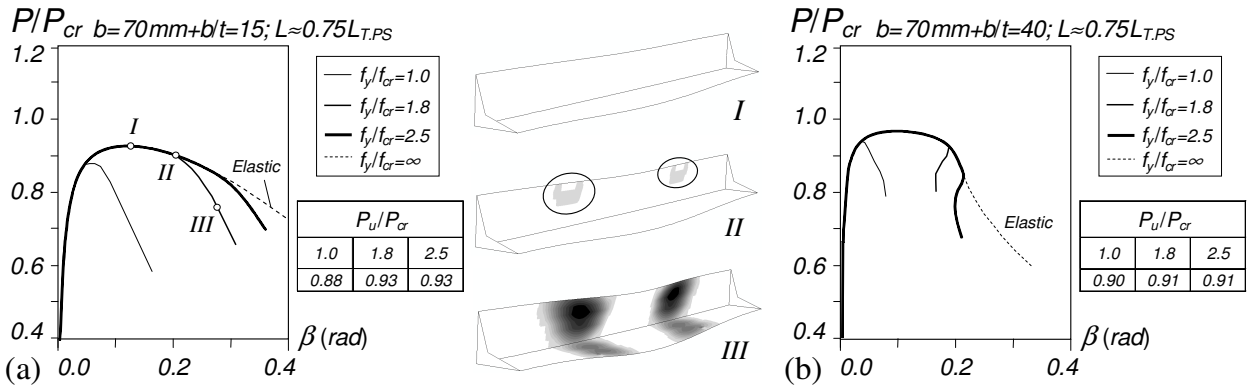

Figure 12: Elastic-plastic equilibrium paths P/P_{cr} *vs.* β (f_y/f_{cr}=1.0; 1.8; 2.5; ∞) for PS columns with $L\approx 0.75\,L_{T.PS}$ and (a) b/t=15 (plastic strain diagram evolution for $f_y/f_{cr}\approx$1.8 column also included) or (b) b/t=40

(v) The different post-buckling behaviors exhibited by the short and intermediate-to-long columns were also observed for slender-leg (cold-formed) F and PC columns ($b/t>20$) – this feature is at the root of the DSM design approach developed specifically for such columns (Dinis & Camotim 2015).

4.3 Imperfection-Sensitivity

This imperfection-sensitivity study consists of comparing the elastic-plastic equilibrium paths and failure loads (P_u) of short ($L\approx 0.25\,L_{T.PS}$) and intermediate-to-long ($L\approx 0.75\,L_{T.PS}$) columns with b=70 mm and stocky legs (b/t=15). They exhibit yield-to-critical stress ratios f_y/f_{cr}=1.0, 1.8, 2.5 and initial geometrical imperfections combining (i) the (critical) FT buckling mode shape, with amplitude equal to 0.1 t, with (ii) the (non-critical) F buckling mode shape, with various (increasing) amplitudes, namely $\pm L/2000$ (F_1), $\pm L/1000$ (F_2), $\pm L/750$ (F_3), $\pm L/500$ (F_4) and $\pm L/250$ (F_5) – positive stands for leg tips under compression. The ultimate-to-critical load ratios P_u/P_{cr} obtained from this imperfection-sensitivity study are given in Table 4 – $P_{u.F+}$ and $P_{u.F-}$ stand for failure loads associated with "positive" and "negative" minor-axis flexural imperfections, respectively. Also given in Table 4 are the percentage differences between these failure load pairs (sharing the same imperfection amplitude): $\Delta=[(P_{u.F-}-P_{u.F+})/P_{u.F+}]\times 100$.

Figs. 13(a)-(b) show the upper parts of the equilibrium paths P/P_{cr} *vs.* d_m/t of short ($L\approx 0.25\,L_{T.PS}$) and intermediate-to-long ($L\approx 0.75\,L_{T.PS}$) columns (i) exhibiting f_y/f_{cr}=1.0, 1.8, 2.5 and (ii) containing the initial geometrical imperfections F_2 ($\pm L/1000$ – value often prescribed in specifications) – note the different horizontal scales (1:5). The observation of these results leads to the following remarks:

(i) The comparison between the equilibrium path shapes and failure loads associated with positive and negative F_2 initial imperfections shows that the influence of this sign is markedly different in the

Table 4: P_u/P_{cr} values of PS columns containing different initial geometric imperfections (amplitude and sign)

Column b/t=15	*Length*																	
	$L\approx 0.25\,L_{T.PS}$			$L\approx 0.75\,L_{T.PS}$														
Imperfection	F_2			F_1			F_2			F_3			F_4			F_5		
f_y/f_{cr}	1.0	1.8	2.5	1.0	1.8	2.5	1.0	1.8	2.5	1.0	1.8	2.5	1.0	1.8	2.5	1.0	1.8	2.5
F^+	0.79	0.91	0.94	0.84	0.90	0.90	0.79	0.87	0.87	0.76	0.85	0.85	0.72	0.81	0.81	0.61	0.73	0.73
F^-	0.81	0.94	0.97	0.90	0.96	0.96	0.83	1.00	1.00	0.79	1.03	1.03	0.73	1.09	1.09	0.62	0.92	1.07
Δ (%)	2.5	3.2	3.2	7.1	6.7	6.7	5.1	14.9	14.9	3.9	21.2	21.2	1.4	34.6	34.6	1.6	26.0	46.6

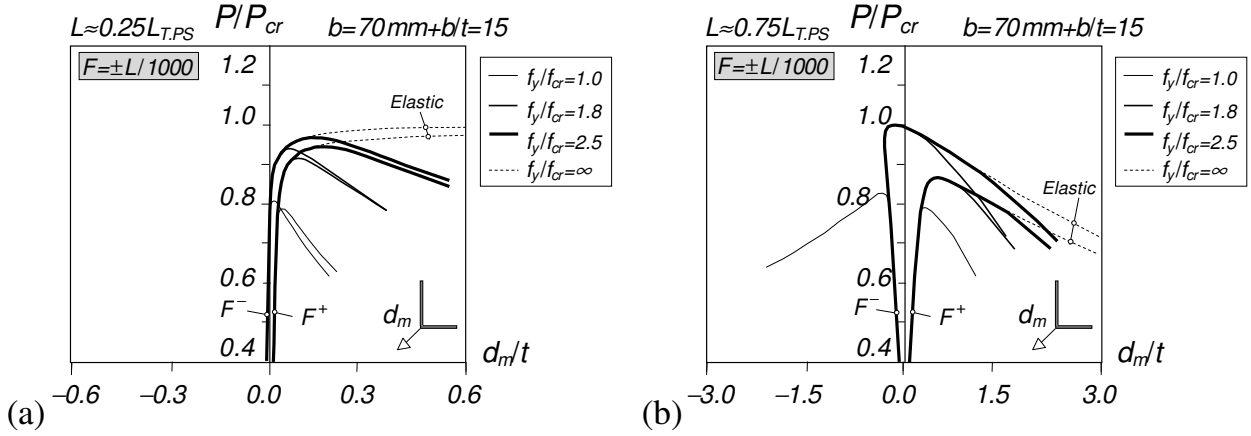

Figure 13: PS column elastic-plastic equilibrium paths P/P_{cr} *vs.* d_m for b=70 mm, b/t=15, f_y/f_{cr}≈1.0, 1.8, 2.5, ∞, F_2 initial geometrical imperfections and lengths (a) $L\approx 0.25\ L_{T.PS}$ or (b) $L\approx 0.75\ L_{T.PS}$

short ($L\approx 0.25\,L_{T.PS}$) and intermediate-to-long ($L\approx 0.75\,L_{T.PS}$) columns: fairly small in the first case and quite relevant in the second one. Naturally, this influence increases with f_y/f_{cr} value in both cases.

(ii) In $L\approx 0.75\,L_{T.PS}$ columns with high yield stresses, the value of Δ can be quite considerable, which means that the initial imperfection sign may alter significantly the column failure load.

(iii) Generally speaking the equilibrium paths P/P_{cr} *vs.* d_m/t evolve towards positive d_m values, regardless of the initial geometrical imperfection sign. Indeed, when such initial imperfection is "negative", the equilibrium paths exhibit a d_m "reversal". In the $L\approx 0.75\,L_{T.PS}$ columns, such "reversal" often occurs at an elastic limit point – the only exception to this "rule" is the column with f_y/f_{cr}=1.0.

(iv) The above behavioral feature stems from the combination of two influences, namely (iv_1) the initial imperfection amplitude and sign, which may cause either positive or negative d_m values, and (iv_2) the minor-axis flexure caused by the effective centroid shift effects due to the redistribution of the leg normal stresses along the equilibrium path (not counteracted by end moments), which always cause positive d_m values. Obviously, these two influences oppose/reinforce each other when the column contains negative/positive initial imperfections. Moreover, and regardless of their sign, the d_m values are "amplified" by the interaction with minor-axis flexural buckling, which becomes gradually more important as the column length approaches $L_{T.PS}$ (closer flexural-torsional and flexural buckling loads) – *i.e.*, is more relevant for the $L\approx 0.75\,L_{T.PS}$ columns than for their $L\approx 0.25\,L_{T.PS}$ counterparts.

(v) For the initial imperfection amplitude considered (L/1000), the effective centroid shift effects quickly become dominant in the $L\approx 0.25\,L_{T.PS}$ columns, even if they are minute – note that there are virtually no interaction effects. Indeed, the (minute) d_m value is already positive for P/P_{cr}=0.5 (even with the enlarged horizontal scale, this is barely visible in the F^- curve of Fig. 13(a)). In the $L\approx 0.75\,L_{T.PS}$ columns, on the other hand, the presence of considerable interaction effects, which quickly amplify the negative d_m values considerably, make it much "harder" for the effective centroid shift effects to "overcome" them. Consequently, the d_m reversal only takes place for $P/P_{cr}\approx 1.0$ and is immediately followed by an elastic limit point, provided that a collapse governed by plasticity has not yet occurred (for the column analyzed, this only happens for f_y/f_{cr}=1.0).

(vi) Naturally, the columns with positive initial imperfections (leg tips under compression) always exhibit lower failure loads. The percentage differences vary between (vi_1) 2.5% (f_y/f_{cr}=1.0) and 3.2% ($f_y/f_{cr}\geq 1.8$), for the $L\approx 0.25\,L_{T.PS}$ columns, and (vi_2) 5.1% (f_y/f_{cr}=1.0) and 14.9% ($f_y/f_{cr}\geq 1.8$), for the $L\approx 0.75\,L_{T.PS}$ columns – as mentioned earlier, the differences are much higher in the latter

case. Note that, in both cases, the failure load takes place in the elastic range for $f_y/f_{cr} \geq 1.8$, which means that the column ultimate strength is not affected by any further increase in the yield stress.

(vii) It is worth investigating the influence of the initial imperfection amplitude and sign on the failure load of intermediate-to-long columns (this influence is quite small in the short columns). This issue, which will be addressed next, is bound to have significant impact on the experimental failure loads of short-to-intermediate angle columns, namely on its scatter, which may become quite high. At this stage, it should be recalled that short-to-intermediate angle columns usually exhibit moderate-to-low slenderness (λ_{fte}) values.

Figs. 14(a)-(d) show the upper parts of the equilibrium paths P/P_{cr} *vs.* d_m/t of $L \approx 0.75\,L_{T.PS}$ columns exhibiting the same f_y/f_{cr} values four additional initial imperfection amplitudes: $L/2000$ (F_1), $L/750$ (F_3), $L/500$ (F_4) and $L/250$ (F_5). The observation of these paths (and Table 4) leads to the following remarks:

(i) The behavioral features exhibited by the columns with $L/1000$ (F_2) initial imperfections remain qualitatively valid, namely the influence of the initial imperfection sign on the failure load.

(ii) Naturally, the failure load of the columns containing positive initial imperfections decreases with their amplitude – for the amplitudes considered in this work, P_u/P_{cr} drops (ii_1) from 0.84 (F_1) to 0.61 (F_5), for $f_y/f_{cr}=1.0$, and (ii_2) from 0.90 (F_1) to 0.73 (F_5), for $f_y/f_{cr} \geq 1.8$.

(iii) In the columns containing negative initial imperfections, it becomes increasingly "difficult" for the effective centroid shift effects to counteract the amplification of the initial imperfections as their

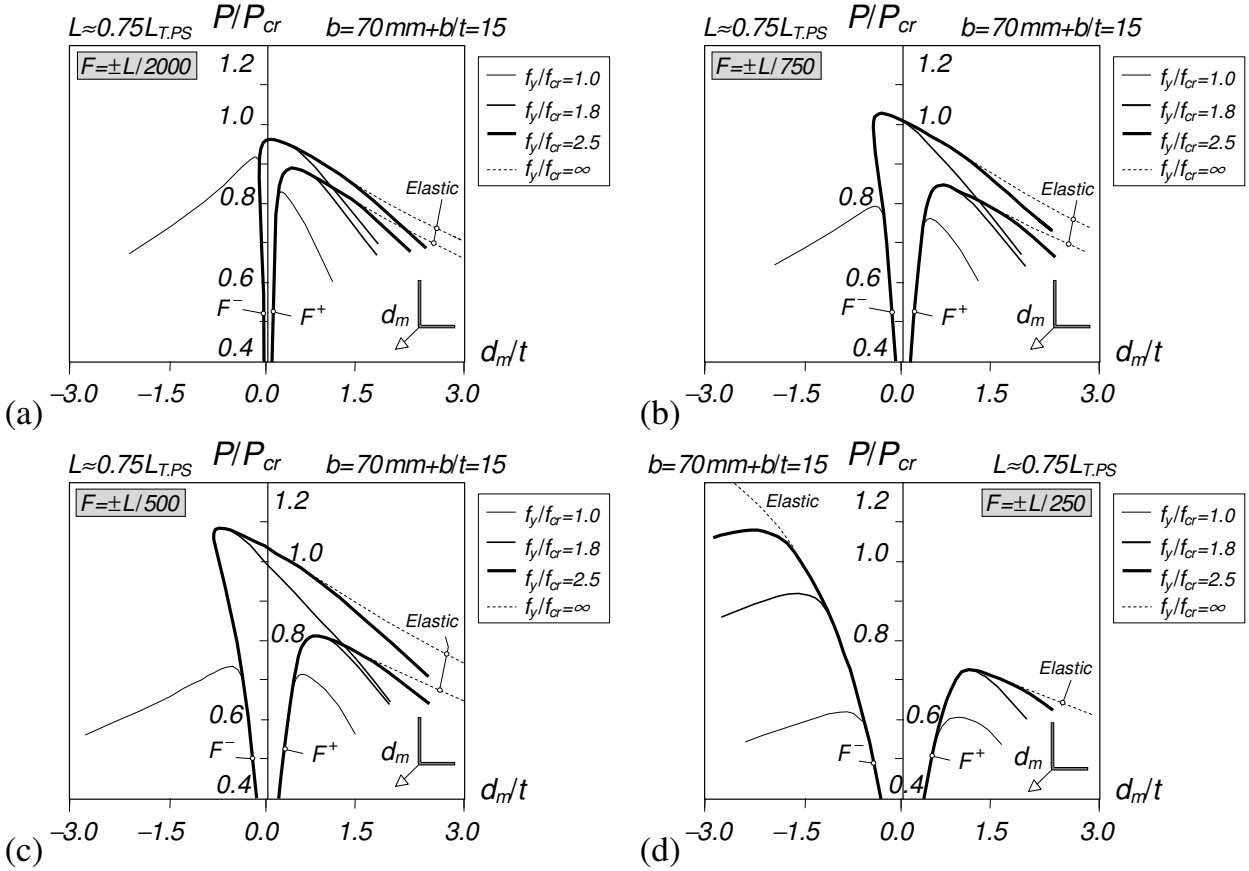

Figure 14: PS $L \approx 0.75\,L_{T.PS}$ column elastic-plastic equilibrium paths P/P_{cr} *vs.* d_m for b=70mm, b/t=15, $f_y/f_{cr} \approx 1.0, 1.8, 2.5, \infty$ and (a) F_1, (b) F_3, (c) F_4 and (d) F_5 initial imperfection amplitudes

amplitude grows. This can be confirmed by the fact that the d_m reversal occurs at higher elastic limit points and associated d_m values – for $L/250$ (F_5), there is even no elastic limit point (see Fig. 14(d)). Moreover, only for f_y/f_{cr}=1.0 does P_u/P_{cr} drop with the initial imperfection amplitude: from 0.90 (F_1) to 0.62 (F_5). Indeed, the opposite happens for higher yield stresses ($f_y/f_{cr}\geq$1.8): P_u/P_{cr} increases with the initial imperfection amplitude – from 0.96 (F_1) to 1.09 (F_5).

(iv) Concerning the Δ value, only for f_y/f_{cr}=1.0 does it decrease monotonically with the initial imperfection amplitude. For higher yield stresses ($f_y/f_{cr}\geq$1.8), Δ grows with the initial imperfection amplitude up to $L/500$ (F_4), *i.e.*, until a d_m reversal still occurs – for f_y/f_{cr}=2.5, it reaches about 35% and is equal to 15% for the commonly adopted $L/1000$ (F_2). Once the d_m reversal ceases to occur (*e.g.*, for $L/250$ (F_5)), the behavior is similar for columns containing positive and negative initial imperfections – see Fig. 15(d). Note that, for $f_y/f_{cr}\geq$1.8, the failure load now drops when the initial imperfection amplitude increases from for $L/500$ (F_4) to for $L/250$ (F_5): either from 1.09 to 0.92 (f_y/f_{cr}=1.8) or from 1.09 to 1.07 (f_y/f_{cr}=2.5) – since there is no longer an elastic limit point, further increasing the yield stress would lead to higher failure loads.

(v) As mentioned earlier, the above large Δ values indicate that the failure loads obtained from an experimental campaign involving short-to-intermediate angle columns may exhibit a high scatter, due to the variation in minor-axis flexural initial imperfection amplitude and (mostly) sign. Such high scatter was observed in the experimental failure loads concerning PC columns (Dinis & Camotim 2015, 2016b) – note that the imperfection-sensitivities of PC and PS columns are similar.

4.4 Residual Stress Effects

It is well known that residual stresses also influence the load-carrying capacity of structural members built from hot-rolled steel profiles – in the case of columns, such influence is often already "embedded" in the design curves appearing in most of the existing codes and specifications. As far as the residual stresses in angle columns are concerned, experimental studies carried out in the 70's led to the practically universal adoption of the 3-point linear diagram depicted in Fig. 15(a) (*e.g.*, ECCS 1976, Ziemian 2010), namely in the current version of Part 1-1 of Eurocode 3 (EC3-1-1 – CEN 2005). However, the fast growing use of high-strength steel to fabricate angle columns with rather wide legs (*e.g.*, b/t=300/35) prompted further experimental investigations aimed at obtaining the residual stress distribution present in these new profiles (*e.g.*, Ban *et al.* 2012, Može *et al.* 2014) – Fig. 15(a) also shows the 4-point linear residual stress distribution proposed by Može *et al.* (2014).

The numerical study presented next is intended to compare the influence of the two residual stress distributions displayed in Fig. 15(a) on the failure load of PS angle columns – $\chi=[(P_u-P_{u.rs})/P_u]\times 100$, where $P_{u.rs}$ and P_u are the failure loads of angle column failure loads with and without residual stresses, is a parameter measuring the failure load drop due to the residual stresses. Fig. 15(b), concerning columns with b=70 mm, b/t=15, $L\approx 0.75\,L_{T.P}$ and f_y=500 MPa, shows illustrative elastic-plastic equilibrium paths P/P_{cr} *vs.* β obtained without (no_rs) and with (rs_3P or rs_4p) residual stresses. Failure load drops of χ= 3.4 % and χ= 0.9 % were observed for the rs_3p and rs_4p columns, respectively. The columns analyzed (i) have geometries defined by b=70 mm, b/t=11, 15, 20 and $L\approx 0.25\,L_{T.PS}, 0.5\,L_{T.PS}, 0.75\,L_{T.PS}$, $L_{T.PS}$, (ii) contain critical-mode initial imperfections with $0.1\,t$ amplitude and (iii) exhibit three yield stresses (f_y= 300, 500, 700 MPa). Note that the stipulation of an unbounded dependency between the maximum residual stress and f_y penalizes the high-strength steel columns, since it is well known that residual stresses in hot-rolled steel profiles are bounded (*e.g.*, Može *et al.* 2014 suggest a maximum value of 70 MPa). Figs. 16(a)-(c) plot the variations of χ with $L/L_{T.PS}$, b/t and $\lambda_{ft}=(f_y/f_{cr.ft})^{0.5}$, respectively. The observation of these failure load results leads to the following remarks:

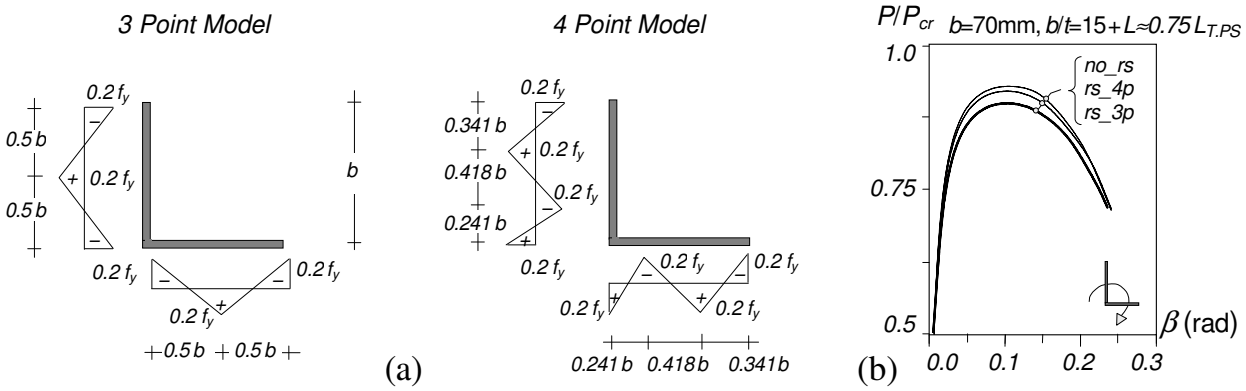

Figure 15: Hot-rolled angle columns: (a) 3- and 4-point residual stress distributions, (b) elastic-plastic equilibrium paths P/P_{cr} *vs.* β for PS columns with b=70 mm, b/t=15, $L\approx 0.75\,L_{T.PS}$ and f_y=500 MPa, with and without residual stresses

(i) The influence of the residual stresses on the column failure load is no more than mildly relevant: only for 7 (out of 36) of the columns analyzed does χ exceed 5%. The 3-point distribution causes higher failure load drops than its 4-point counterpart – 4.0% vs. 1.5%. However, note that the first value is almost 2% higher than that obtained for F columns (Dinis *et al.* 2016) and 1% lower than that obtained for PC columns (Dinis & Camotim 2016a) – see Figs. 3(a)-(b).

(ii) The failure load drops higher than 5% (3-point residual stress distributions) occur for intermediate-to-long columns ($L/L_{T.PS}\approx 0.50, 0.75, 1.0$), *i.e.*, columns more prone to interaction between flexural-torsional and flexural buckling (their equilibrium paths exhibit well defined limit points – see Figs. 9(a)-(b)). In addition, note that the highest failure load drops correspond to columns with slenderness below 1.0, which is accordance with the current knowledge.

In view of the fairly similar failure loads obtained with the two residual stress distributions, and since the 3-point one has been used for a long time, it was decided to adopt it also in the parametric study presented next for hot-rolled steel angles. As shown in Figs. 16(a)-(c), such decision is on the safe side, since it leads to lower failure loads. On the other hand, it is well known that residual stresses and rounded corner effects have little impact on the cold-formed steel angle column failure loads – *e.g.*, Ellobody & Young (2005).

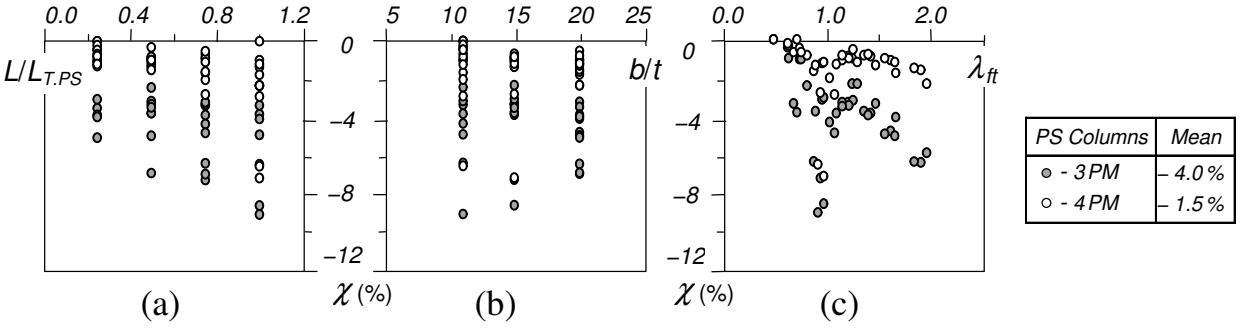

Figure 16: Hot-rolled steel PS angle columns: plots (a) χ vs. $L/L_{T.PS}$, (b) χ vs. b/t, (c) χ vs. λ_{ft}

5. PS Column Failure Load Data

In order to assess whether the DSM design approach developed in the context of cold-formed steel F and PC angle columns is also applicable to PS columns with stocky (hot-rolled steel angles – HRS angles) or slender (cold-formed steel angles – CFS angles) legs, it is necessary to assemble a reasonably large column failure load data, comprising (i) experimental failure loads reported in literature and (ii) numerical

failure loads determined by means of ABAQUS SFEA (employing the model developed earlier, also used to obtain the results presented in the previous sections).

5.1 Experimental Failure Loads

The experimental results gathered concern only HRS PS columns – to the authors' best knowledge, the only CFS angle column test results available are due to Madugula *et al*. (1983), but all the specimens buckle in minor-axis flexural modes, *i.e.*, fall outside the scope of this work. Therefore, the experimental failure loads collected concern (i) 4 column tests by Wakabayashi & Nonaka (1965), with b/t=12.9, (ii) 4 column tests by Kennedy & Murty (1972), with $18.5 \geq b/t \geq 12.8$, (iii) 7 column tests by Kitipornchai & Lee (1986), with $15.9 \geq b/t \geq 13.3$, (iv) 3 column tests by Adluri & Madugula (1996), with $15.8 \geq b/t \geq 12.9$, (v) 9 column tests by Fan (2009), with $16.0 \geq b/t \geq 12.5$, and (vi) 57 column tests by Ban *et al*. (2013), with $16.0 \geq b/t \geq 14.0$ – the tests by Al-Sayed & Bjorhovde (1989) were excluded because they all buckle in minor-axis flexural modes. Therefore, a total of 84 experimental failure loads are available, a number deemed acceptable to assess the merits of the proposed DSM-based design approach for PS angle columns. The specimen cross-section dimensions, lengths L, yield stresses f_y and ultimate strengths f_u are given in Annex A – detailed accounts of the experimental studies can be found in the above publications.

5.2 Numerical Failure Loads

The parametric study carried out involved steel (E=210 GPa, ν=0.3) PS columns with the cross-section dimensions and lengths given in Tables 1 and 2 – the rounded corners were disregarded. The columns considered have lengths and yield stresses (elastic-perfectly plastic material model) selected to ensure (i) buckling in flexural-torsional (predominantly torsional) modes and (ii) covering a wide slenderness range – the yield stresses adopted are 150, 300, 500, 700 MPa. Two sets of 144 short-to-intermediate columns with stocky or slender legs (HRS and CFS columns, respectively) are analyzed, all containing initial geometrical imperfections combining (i) a critical flexural-torsional component, with amplitude equal to 10% of the wall thickness t, and (ii) a non-critical minor-axis flexural component, with amplitude equal to L/1000 (leg tips under compression – most detrimental situation, as unveiled in the previous imperfection-sensitivity study investigation), value commonly adopted in HRS columns (*e.g.*, Može *et al*. 2014) and in line with the measurements reported for CFS columns by Popovic *et al*. (1999). While 3-point residual stress distributions (see Fig. 15(a)) were included in the HRS column analyses, residual stress and corner enhancement effects were disregarded in the CFS columns, since they were found to have little impact on the failure loads (Ellobody & Young 2005, Shi *et al.* 2012). The ultimate strengths (f_u) obtained are presented, in tabular form, in Annexes B (HRS columns) and C (CFS columns).

6. Direct Strength Method (DSM) Design Considerations

The use of the Direct Strength Method (DSM) to design cold-formed steel angle columns has attracted the attention of a few researchers in the past: (i) Young (2004), for F columns, (ii) Rasmussen (2006), for PC columns, and Silvestre *et al*. (2013), for both F and PC fixed columns, put forward DSM-based design approaches based on the combined use of global and local strength curves to obtain ultimate strength estimates (f_{nle}). Even if these design approaches were found to predict the available failure load data quite adequately, the fact they are mostly empirical (the length-dependence of the column post-buckling and failure behaviors is never explicitly taken into account) led Dinis & Camotim (2015) to propose a more rational DSM-based design approach for F and PC columns with slender legs (b/t>20), which was subsequently slightly modified and simplified (Landesmann *et al.* 2016, Dinis & Camotim 2016b). The main features of this design approach are the following:

(i) Based on the fact that most short-to-intermediate angle columns fail in interactive modes combing major-axis flexural-torsional and minor-axis flexural deformations.

(ii) Involves the use of (ii_1) the currently codified DSM global design curve (f_{ne}) and (ii_2) a set of genuine flexural-torsional strength curves (f_{nft}), developed in the context of columns with fully prevented minor-axis bending displacements. These strength curves, useful to design both F and PC columns, make it possible to capture the progressive drop of the column post-critical strength as its length increases along the $f_{cr}(L)$ curve "horizontal plateau".

(iii) The effective centroid shift effects (Young & Rasmussen 1999), strongly affecting the PC column failure loads (not the F ones), are included in the design approach through a coefficient β, which also reflects the change in column flexural-torsional post-buckling behavior along the $f_{cr}(L)$ curve plateau.

(iv) The length dependence of the column flexural-torsional post-critical strength and effective centroid shift effects is quantified by means of the aforementioned parameter $\Delta_f=[(f_{bt}-f_{crft})/f_{bt}]\times 100$, with f_{bt} and f_{crft} obtained from Eq. (1) – see the comments to Fig. 6.

The fruit of the above research effort was a DSM-based design approach (f_{nfte}) for F and PC short-to-intermediate angle columns, which can be cast in the form

$$f_{nfte}=\begin{cases}\beta\cdot f_{ne} & if \quad \lambda_{fte}\le\left(0.5+\sqrt{0.25-b}\right)\frac{1}{2a}\\ \beta\cdot f_{ne}\left(\frac{f_{crft}}{f_{ne}}\right)^{a}\left[1-b\left(\frac{f_{crft}}{f_{ne}}\right)^{a}\right] & if \quad \lambda_{fte}>\left(0.5+\sqrt{0.25-b}\right)\frac{1}{2a}\end{cases} \quad \text{with} \quad \lambda_{fte}=\sqrt{\frac{f_{ne}}{f_{crft}}} \quad , \tag{6}$$

$$a=\begin{cases}0.001\,\Delta_f^3-0.032\,\Delta_f^2+0.250\,\Delta_f+0.400 & if \quad \Delta_f\le 5.0\\ 0.001\,\Delta_f+0.970 & if \quad \Delta_f>5.0\end{cases} \quad , \tag{7}$$

$$b=\begin{cases}0.014\,\Delta_f+0.150 & if \quad \Delta_f\le 7.0\\ 0.248 & if \quad \Delta_f>7.0\end{cases} \quad , \tag{8}$$

$$\beta=\begin{cases}1 & for\ F\ columns\\ \dfrac{0.68}{(\lambda_{fte}-c)^{d}}\le 1 & for\ PC\ columns\end{cases} \quad , \tag{9}$$

$$c=\begin{cases}-300.0\,\Delta_f^3+110.0\,\Delta_f^2-12.8\,\Delta_f+1.0 & if \quad \Delta_f\le 0.2\\ -0.002\,\Delta_f^2-0.200\,\Delta_f+0.480 & if \quad 0.2<\Delta_f<5.0\\ 0.001\,\Delta_f-0.565 & if \quad \Delta_f\ge 5.0\end{cases} \quad , \tag{10}$$

$$d=\begin{cases}380.0\,\Delta_f^3-140.0\,\Delta_f^2+15.2\,\Delta_f+0.25 & if \quad \Delta_f\le 0.2\\ -0.008\,\Delta_f^2+0.094\,\Delta_f+0.712 & if \quad 0.2<\Delta_f<5.0\\ 0.001\,\Delta_f+0.977 & if \quad \Delta_f\ge 5.0\end{cases} \quad , \tag{11}$$

6.1 Application of the Design Approach Proposed in Dinis & Camotim (2015) to PS Columns

Attention is now turned to assessing the performance of Eqs. (6)-(11) in predicting the experimental and numerical column failure loads gathered in this work, which involve HRS and CFS short-to-intermediate lengths columns with spherically-hinged support conditions. The observation of the averages, standard deviations and maximum/minimum values of the failure-to-predicted strength ratios (f_u/f_{nfte}), which are summarized in Table 5, prompts the following remarks:

(i) All available experimental (RHS columns) and numerical (HRS and CFS) failure loads are severely underestimated: f_u/f_{nfte} means and standard deviations equal to 2.15/0.69 (RHS – experimental), 1.76/0.53 (RHS – numerical) and 1.96/0.44 (CFS – numerical).

(ii) The excessively safe and scattered predictions are due to the fact that (ii_1) the PS and F/PC column flexural-torsional buckling curves are markedly different (see Figs. 5(a)-(b)) and (ii_2) because the length dependence of f_{nft} and β is based on parameter Δ_f, whose values are quite different for PC and PS columns – *e.g.*, in the angle columns dealt with in Fig. 6, Δ_f equals 2.5% and 10.9% for the PC and PS columns with lengths $L \approx L_{T.PC}$ and $L \approx L_{T.PS}$, respectively – note that the two transition lengths ($L_{T.PC}$ and $L_{T.PS}$) are quite similar.

(iii) In view of the content of the above item, it is indispensable to develop new flexural-torsional (f_{nft}) and reduction factor (β) curves specifically for PS columns – this will be done in the next section.

Table 5: HRS and CFS short-to-intermediate angle columns: mean, standard deviation and maximum/minimum values of the experimental and numerical failure-to-predicted load ratios concerning the proposal of Dinis & Camotim (2015)

	HRS columns		CFS columns
	Experimental	Numerical	Numerical
Mean	2.15	1.76	1.96
Sd. Dev.	0.69	0.53	0.44
Max	3.51	2.51	2.70
Min	0.92	0.94	1.24

6.2 Modifications of the Proposal of Dinis & Camotim (2015) to Cover PS columns

The DSM design approach for spherically-hinged equal-leg angle columns is based on exactly the same concepts and procedures adopted for F and PC short-to-intermediate angle columns with slender legs (Dinis & Camotim 2015) and later, exclusively on the basis of numerical failure loads, found to handle also columns with stocky legs and containing realistic residual stresses (Dinis *et al.* 2016, Dinis & Camotim 2016a). A fully numerical approach is again adopted to determine new length-dependent (i) flexural-torsional strength curves f_{nft} and (ii) curves providing the reduction coefficient β. Both curves are qualitatively similar to those obtained in the context of F and PC columns: "Winter-type" curves that depend on the length via parameter Δ_f – for Δ_f=0, the new f_{nft} curve coincides with the currently codified DSM local curve and the new β curves coincides with that proposed by Rasmussen (2006). The modifications, with respect to the proposal of Dinis & Camotim (2015), consist of new expressions for the functions $a(\Delta_f)$, $b(\Delta_f)$, $c(\Delta_f)$ and $d(\Delta_f)$. Those differences stem from the fact that the new curves concern columns (i) pinned with respect to major-axis flexure, (ii) fixed with respect to torsion and (iii) with the minor-axis flexural displacements prevented – see Fig. 17(a).

6.2.1 Flexural-torsional strength curves for PS columns

In order to obtain a set of "Winter-type" strength curves intended to predict, as accurately as possible, "pure flexural-torsional failures" of PS equal-leg angle columns, the first step consists of gathering a

fairly large flexural-torsional failure load data, to be subsequently used in the development and validation of the sought strength curves. This is done by determining the failure loads of 100 PS columns continuously restrained against minor-axis flexure, *i.e.*, "forced" to fail in a combination of major-axis flexure and torsion. All the columns analyzed exhibit (i) three slender-leg cross-sections (50×1.2mm, 70×1.2mm, 90×2.5mm – b/t=42,58,36, respectively), (ii) various lengths (all falling inside the $P_{cr}(L)$ curve plateau and such that $0.94 \geq L/L_{T.PS} \geq 0.32$), (iii) critical-mode initial imperfections with amplitude equal to L/1000 and (iv) a large number of yield stresses f_y, ranging from 30 to 1200MPa and selected to ensure covering a wide flexural-torsional slenderness (λ_{ft}) range. Fig. 17(b) plots the obtained ultimate strength ratios f_u/f_y against λ_{ft} – also depicted in this figure is the current DSM local strength curve, clearly unable to predict all the failure loads.

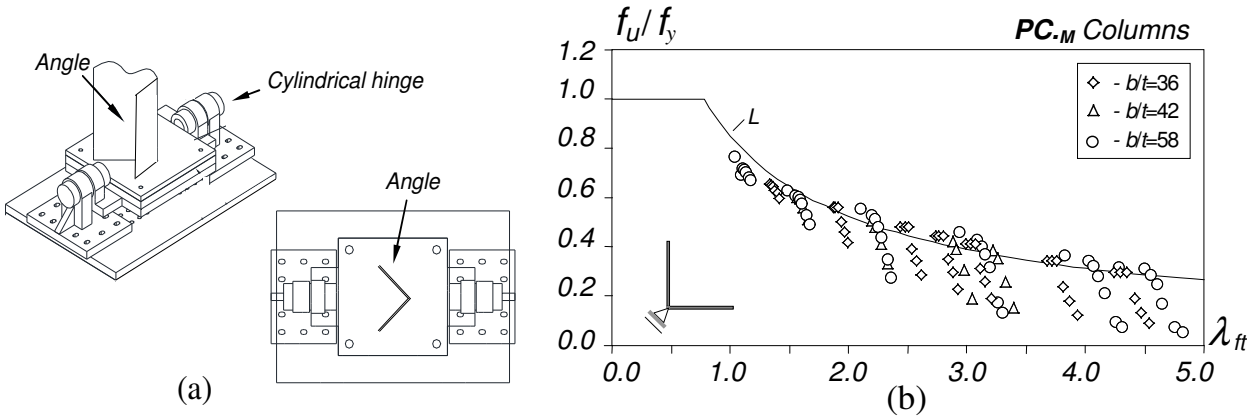

Figure 17: (a) Schematic representation of the restrained PS column support condition (3D and top views) nad (b) plots of f_u/f_y vs. λ_{ft} for all the restrained columns analyzed in this work

Then, after grouping the columns according to their Δ_f value, it possible to obtain, through a "trial-and-error curve-fitting procedure" based on the available numerical failure load data, expressions for the functions $a(\Delta_f)$ and $b(\Delta_f)$, which read

$$a = \begin{cases} -0.001\ \Delta_f^3 + 0.014\ \Delta_f^2 - 0.007\ \Delta_f + 0.4 & if \quad \Delta_f \leq 1 \\ 0.001\ \Delta_f^2 + 0.04\ \Delta_f + 0.365 & if \quad 1 < \Delta_f < 10 \\ 0.865 & if \quad \Delta_f \geq 10 \end{cases}, \tag{12}$$

$$b = \begin{cases} -0.001\ \Delta_f^3 + 0.001\ \Delta_f^2 - 0.011\ \Delta_f + 0.15 & if \quad \Delta_f \leq 1 \\ 0.005\ \Delta_f + 0.134 & if \quad 1 < \Delta_f < 10 \\ 0.184 & if \quad \Delta_f \geq 10 \end{cases}. \tag{13}$$

Figs. 18(a)-(d) plot f_u/f_y (white dots) and f_{nft}/f_y (grey dots) against λ_{ft} for columns with $\Delta_f \approx 0.5$, $\Delta_f \approx 1.8$, $\Delta_f \approx 5.0$ and $\Delta_f \approx 9.8$, respectively – also depicted in this figure are the flexural-torsional strength curves obtained from Eqs. (6), (12) and (13) for Δ_f=0.5,1.8,5.0,9.8. The observation of these results shows that the three curves shown in Figs. 18(a)-(d) follow the numerical failure load trends reasonably well, in the sense that they provide more or less accurate underestimations of their values.

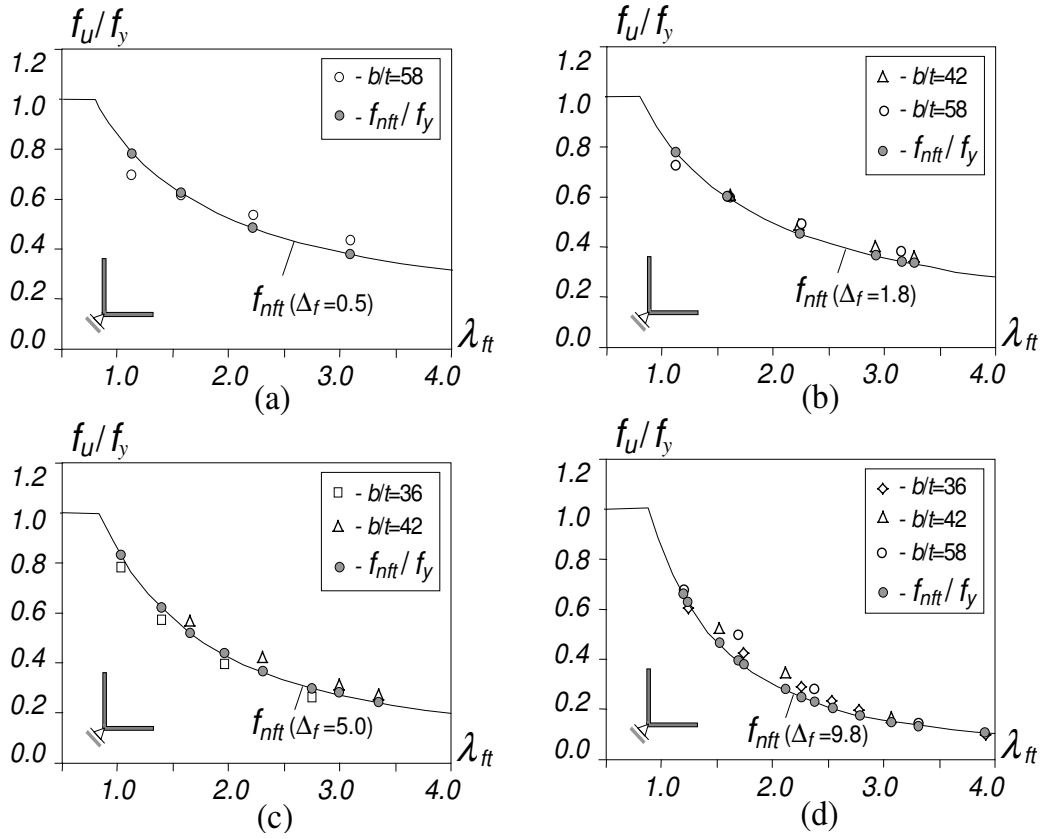

Figure 18: Plots of f_u/f_y against λ_{ft} and proposed flexural-torsional strength curves for (a) Δ_f=0.5, (b) Δ_f=1.8, (c) Δ_f=5.0, (d) Δ_f=9.8

6.2.2 Reduction coefficient (β) for PS columns

The procedure adopted to search for an expression providing the function $\beta(\Delta_f)$ is based on an "elastic reduction factor" concept and involves the following steps:

(i) Perform elastic post-buckling analyses of geometrically identical restrained and unrestrained PS columns (sharing the same critical-mode initial geometrical imperfections with amplitude $L/1000$) and record the evolution, as the applied load increases, of the maximum longitudinal normal stresses (f_{max}), occurring at the mid-span cross-section. For illustrative purposes, Fig. 19(a) displays the P vs. f_{max} curves concerning restrained (PS_R) and unrestrained (PS) columns with b/t=58 and Δ_f=0.5.

(ii) Assume that, for a given f_{max} value, the difference between the PS_R and PS column applied loads (P_{PSR} and P_{PS}) stems exclusively from the effective centroid shift effects – then, the P_{PS}/P_{PSR} ratio provides a good approximation for β (*i.e.*, it is assumed that $\beta \approx P_{PS}/P_{PSR}$).

(iii) Relate f_{max} with the column slenderness by means of $\lambda_{ft}=(f_{max}/f_{crft})^{0.5}$, which amounts to assuming that β is the strength reduction due to the effective centroid shift effects at the "elastic limit state".

(iv) By means of another "trial-and-error curve-fitting procedure", look for the expressions for the functions $c(\Delta_f)$ and $d(\Delta_f)$ – for illustrative purposes, Fig. 19(b) displays the curves concerning the columns with Δ_f=0.5, 5.0, 9.8. The best approximations were found to be

$$c = \begin{cases} -300\ \Delta_f^3 + 110\ \Delta_f^2 - 12.8\ \Delta_f + 1 & \text{if} \quad \Delta_f \le 0.2 \\ -0.001\ \Delta_f^3 + 0.01\ \Delta_f^2 - 0.058\ \Delta_f + 0.451 & \text{if} \quad 0.2 < \Delta_f < 8 \\ 0.115 & \text{if} \quad \Delta_f \ge 8 \end{cases}, \tag{14}$$

$$d = \begin{cases} 290\ \Delta_f^3 - 98\ \Delta_f^2 + 10.8\ \Delta_f + 0.25 & if \quad \Delta_f \le 0.2 \\ -0.001\ \Delta_f^2 + 0.03\ \Delta_f + 0.804 & if \quad 0.2 < \Delta_f < 9.5 \\ 0.999 & if \quad \Delta_f \ge 9.5 \end{cases} \qquad (15)$$

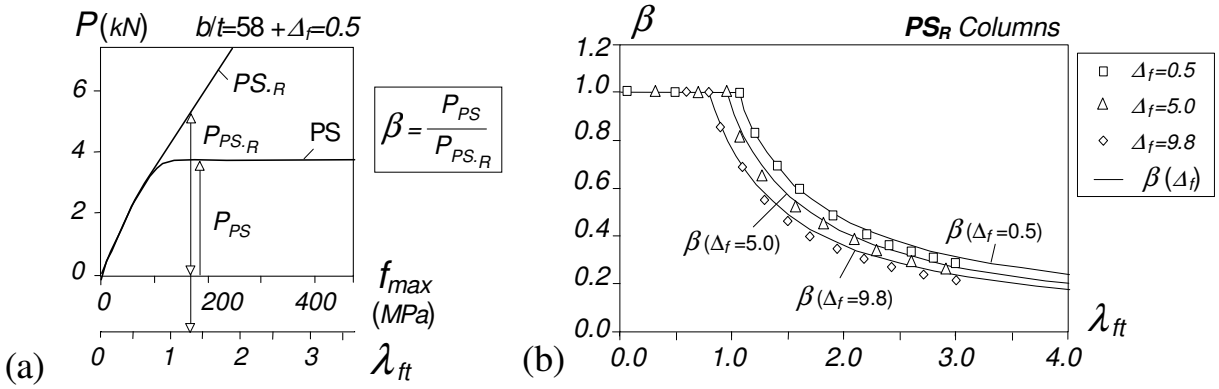

Figure 19: (a) P vs. f_{max} curves for PS_R and PS columns (Δ_f=0.5), and (b) numerically obtained $\beta(\lambda_{ft})$ curves and comparison with the numerical values for PS columns with Δ_f=0.5, 5.0, 9.8

6.3 Assessment of the Proposed DSM-Based Design Approach for PS Columns

In order to assess the performance/merits of the proposed/modified DSM-based design approach, one considers next the predictions (f_{nfte}) of the whole set of experimental (HRS columns) and numerical (HRS and CFS columns) failure loads, which are given in the tables included in Annexes A-C – while Annex A concerns the experimental values, Annexes B and C deal with the numerical ones. The above tables also include the failure-to-predicted strength ratios f_u/f_{nfte} associated with these failure loads. Moreover, the prediction quality is also assessed through the determination of the Load and Resistance Factor Design (LRFD) resistance factor associated with the estimates of the proposed/modified DSM design approach. In particular, it is intended to check whether a factor equal or higher than ϕ_c=0.85 is obtained – this is the value recommended, for compression members, by the current North American Specification (AISI 2016) – according to this specification (Chapter K – Section K2.1.1), ϕ_c can be calculated by means of the expression

$$\phi_c = C_\phi (M_m F_m P_m)\, e^{-\beta_0 \sqrt{V_M^2 + V_F^2 + C_P V_P^2 + V_Q^2}} \qquad \text{with} \qquad C_P = \left(1 + \frac{1}{n}\right)\frac{m}{m-2} \quad , \qquad (16)$$

where (i) C_ϕ is a calibration coefficient (C_ϕ=1.52 for LRFD), (ii) M_m=1.10 and F_m=1.00 are the mean values of the material and fabrication factors, respectively, (iii) β_0 is the target reliability index (β_0=2.5 for structural members in LRFD), (iv) V_M=0.10, V_F=0.05 and V_Q=0.21 are the coefficients of variation of the material factor, fabrication factor and load effect, respectively, (v) C_P is a correction factor depending on the numbers of tests (n) and degrees of freedom (m=n-1), and (vi) P_m and V_P are the mean and standard deviation of the "exact"-to-predicted ultimate strength ratios f_u/f_{nfte}.

Figs. 20(a)-(b) plot the f_u/f_{nfte} ratios against λ_{fte} for the whole set of HRS (experimental and numerical) and CFS (numerical) angle column ultimate strengths – the associated averages, standard deviations and maximum/minimum values are also included in these figures. Table 6 shows the n, P_m, V_P and ϕ_c values associated with the application of the proposed/modified DSM design approach to the spherically-hinged

angle column numerical, experimental and numerical+experimental failure loads reported in this work. The observation of these results prompts the following remarks:

(i) The proposed DSM design approach leads to quite accurate predictions of the experimental and numerical ultimate strengths: the f_u/f_{nfte} averages and standard deviations are (i_1) 1.16/0.19 (HRS experimental data), (i_2) 1.01/0.08 (HRS numerical data) and (i_3) 1.06/0.08 (CFS numerical data).

(ii) The higher scatter of the HRS experimental failure load predictions is easily explained by the very high sensitivity of the column ultimate strength to the minor-axis flexural initial imperfection (sign and amplitude) – see Section 4.3. Indeed, the observation of Figs. 21(a)-(b), which plot the experimental f_u/f_{nfte} ratios against the column length L and $L/L_{T.PS}$ ratio, shows that (ii_1) the highest ultimate strength overestimations occur for the longer columns and (ii_2) the scatter increases with the column $L/L_{T.PS}$ ratio – recall that it was found that the column imperfection-sensitivity increases significantly with this ratio.

(iii) The quality of the above failure load predictions is very similar to that found by Dinis & Camotim (2015) for the cold-formed steel PC angle columns: f_u/f_{nfte} average/standard deviation of 1.13/0.25

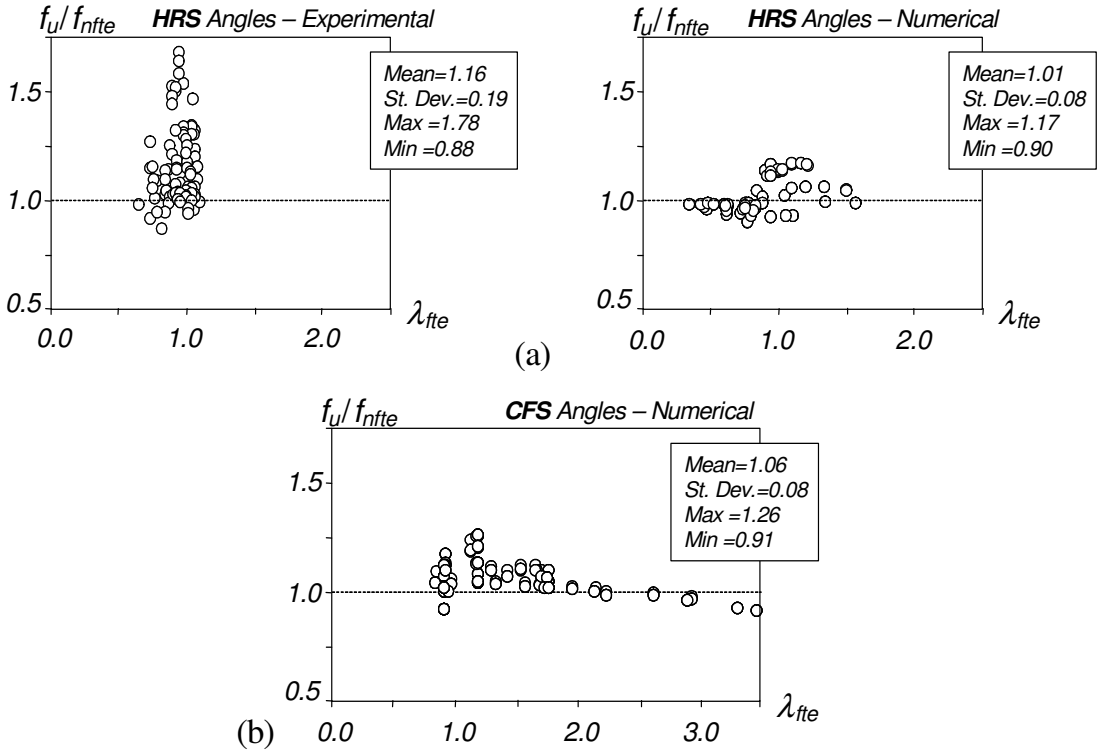

Figure 20: Plots of f_u/f_{nfte}, against λ_{fte}, for the (a) HRS and (b) CFS angle columns

Table 6: Hot-rolled and cold-formed steel angle columns: LRFD resistance factors ϕ calculated according to AISI (2016)

	HRS angles			CRS angles
	Experimental	Numerical	Both	Numerical
n	84	144	228	144
P_m	1.162	1.010	1.066	1.058
V_P	0.192	0.076	0.150	0.081
ϕ_c	0.90	0.90	0.88	0.94

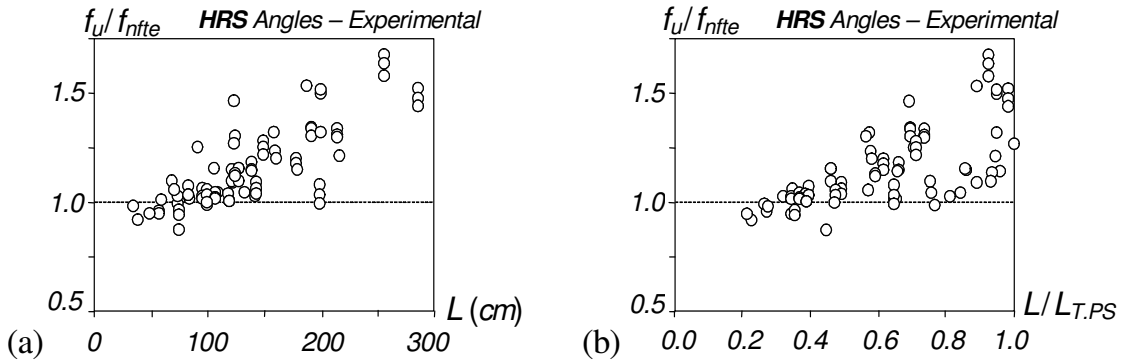

Figure 21: HRS angle column experimental results: plots of f_u/f_{nfte} against (a) length L and (b) $L/L_{T.PS}$ ratio

(experimental data) and 1.10/0.09 (numerical data). Therefore, it may be safely argued that this prediction quality provides solid evidence concerning the adequacy of the reasoning behind the development of the flexural-torsional strength and β vs. λ_{fte} curves, which reflect quite accurately the underlying mechanical features.

(iv) The resistance factors associated with the application of the proposed DSM design approach are ϕ_c=0.88 (HRS columns – experimental and numerical failure loads) and ϕ_c=0.94 (CFS columns – numerical failure loads). These ϕ_c values exceed the one recommended in AISI (2016) – ϕ_c=0.85.

(v) Finally, it seems fair to conclude that the proposed DSM design approach provides high-quality predictions of the whole set of experimental and numerical PS column failure loads collected and obtained in this work. However, it is indispensable to have additional validation of the proposed design procedure, involving both experimental (mostly) and numerical results. In particular, note that (to the authors' best knowledge, of course), (v_1) there are no experimental failure loads for CFS columns and (v_2) the available HRS column failure loads correspond to a quite narrow and fairly low λ_{fte} slenderness range.

7. Conclusion

This work dealt with the structural behavior, strength and DSM design of spherically-hinged (simply supported) short-to-intermediate equal-leg steel columns, thus extending the scope of similar studies recently carried out by the authors for fixed and cylindrically-hinged (simply supported) columns with the same characteristics – hot-rolled (stocky legs – b/t<20) and cold-formed (slender legs – b/t≥20) are dealt with separately. After briefly reviewing the most relevant findings unveiled in recent works, concerning fixed and cylindrically-hinged columns, a numerical investigation on the buckling, post-buckling (elastic and elastic-plastic) and strength of these columns was reported – the numerical results presented and discussed, which included the selection of the column geometries to be analyzed, were obtained by means of GBT (buckling) and ABAQUS shell finite element (post-buckling) analyses. Next, the paper addressed the geometrically and materially non-linear behavior of columns containing initial geometrical imperfections (mostly minor-axis flexural ones) and/or residual stresses – special attention was paid to (i) the performance of an imperfection-sensitivity study, which unveiled quite surprising (non intuitive) findings, and (ii) the modeling the residual stresses in hot-rolled steel angle columns. It became possible to conclude that there are key behavioral features shared by hot-rolled (stocky legs) and cold-formed (slender legs) steel angle columns, namely (i) the strong and length-dependent (i_1) interaction between major-axis flexural-torsional and minor-axis buckling, and (i_2) effective centroid shift effects, and (ii) the reduced impact of the residual stresses on the column failure load – such features are also shared by the fixed and cylindrically-hinged angle columns investigated earlier. Then, the paper

addressed (i) the literature search carried out, aimed at finding experimental angle column failure loads, and (ii) the performance of a parametric study, intended to obtain a fairly large set of numerical angle column failure loads, covering a wide slenderness range. Finally, after confirming that the existing DSM design approach, valid for fixed and cylindrically-hinged cold-formed steel columns, cannot be readily applied to their spherically-hinged counterparts (the change in major-axis flexure end support conditions strongly influences the column ultimate strength), a new design approach was developed on the basis of similar concepts and procedures – in fact, it can be viewed as a (slight) modification of the previous one. The modified/proposed DSM design approach, involving new (length-dependent) flexural-torsional strength and reduction factor curves, was shown to yield safe and reliable failure load estimates for both hot-rolled and cold-formed columns buckling in flexural-torsional modes. In particular, the failure load predictions provided lead to LRFD resistance factors higher than ϕ_c=0.85 (value recommended by the current North American specification for compression members). Nevertheless, additional nujmerical and experimental validation is indispensable before the above design approach reaches the codification stage – in particular, experimental results concerning cold-formed steel columns are heavily needed.

References

Adluri S.M.R., Madugula M.K.S. (1996). Flexural buckling of steel angles: Experimental investigation, *Journal of Structural Engineering* (ASCE), **122**(3), 309–317.

AISI (American Iron and Steel Institute) (2016). *North American Specification (NAS) for the Design of Cold-Formed Steel Structural Members* (AISI-S100-16), Washington DC.

Al-Sayed S.H., Bjorhovde R. (1989). Experimental study of single angle columns, *Journal of Constructional Steel Research*, **12**(2), 83-102.

ArcelorMittal (2015). *ArcelorMittal Sections*, http://www.arcelormittal.com/sections/en.

Ban H., Shi G., Shi Y. Wang Y. (2012). Residual stress tests of high-strength steel equal angles, *Journal of Structural Engineering* (ASCE), **138**(12), 1446-1454.

Ban H.Y., Shi G., Shi Y.J., Wang Y.Q. (2013). Column buckling tests of 420 MPa high strength steel single equal angles, *International Journal of Structural Stability and Dynamics*, **13**(2), 1-23.

Bebiano R., Pina P., Silvestre N., Camotim D. (2008). *GBTUL 1.0β – Buckling and Vibration Analysis of Thin-Walled Members*, DECivil/IST, Technical University of Lisbon. (http://www.civil.ist.utl.pt/gbt)

Camotim D., Dinis P.B., Martins A.D. (2016). Direct strength method (DSM) – a general approach for the design of cold-formed steel structures, *Recent Trends in Cold-Formed Steel Construction*, C. Yu (ed.), Woodhead Publishing (Series in Civil and Structural Engineering), Amsterdam, 69-105.

Comité Européen de Normalisation (CEN) (2005). *Eurocode 3, Design of Steel Structures – Part 1-1: General Rules and Rules for Buildings*, Brussels, Belgium, 2005.

Dinis P.B., Camotim D. (2015). A novel DSM-based approach for the rational design of fixed-ended and pin-ended short-to-intermediate thin-walled angle columns, *Thin-Walled Structures*, **87**(February), 158-182.

Dinis P.B., Camotim D. (2016a). Behavior and design of hot-rolled steel pin-ended short-to-intermediate angle columns, *USB Key Drive Proceedings of Seventh International Conference on Coupled Instabilities in Metal Structures* (CIMS 2016 – Baltimore, 7-8/11), Paper 23.

Dinis P.B., Camotim D. (2016b). Proposal for the codification of a DSM design approach for cold-formed steel short-to-intermediate angle columns, *Proceedings of Wei-Wen Yu International Specialty Conference on Recent Research and Developments in Cold-Formed Steel Structures* (Baltimore, 9-10/11), R. LaBoube, W.-W. Yu (eds.). 155-171.

Dinis P.B., Camotim D., Silvestre N. (2012). On the mechanics of angle column instability, *Thin-Walled Structures*, **52**(March), 80-89.

Dinis P.B., Camotim D., Silvestre N. (2007). FEM-based analysis of the local-plate/distortional mode interaction in cold-formed steel lipped channel columns, *Computers & Structures*, **85**(19-20), 1461-1474.

Dinis P.B., Camotim D., Preto V. (2016). Behaviour and design of short-to-intermediate hot-rolled steel angle columns, *Proceedings of the International Colloquim on Stability and Ductility of Steel Stuctures* (SDSS 2016 – Timisoara, 30/5 to 1/6), D. Dubina, V. Ungureanu (eds.), Wiley/Ernst & Sohn (Mem Martins), 477-484.

Ellobody E, Young B (2005). Behavior of cold-formed steel plain angle columns, *Journal of Structural Engineering* (ASCE), **131**(3), 469-478.

European Convention for Constructional Steelwork (ECCS) (1976). *Manual on Stability of Steel Structures*, ECCS, Brussels.

Fan J.K. (2009). *Theoretical and Experimental Study on Q460 Single Equal-Leg Angles under Axial Compression*, Master Thesis, Xian University of Architecture and Technology, Xian, China.

Kennedy J.B., Murty M.K.S. (1972). Buckling of steel angle and tee struts, *Journal of the Structural Division* (ASCE), **98**(11), 2507-2521.

Kitipornchai S., Lee H.W. (1986). Inelastic experiments on angle and tee struts, *Journal of Constructional Steel Research*, **6**(3), 219–236.

Landesmann A., Camotim D., Dinis P.B., Cruz R. (2016). Short-to-intermediate slender pin-ended cold-formed steel equal-leg angle columns: experimental investigation, numerical simulations and DSM Design, *Engineering Structures*, **132**(1 February), 471-493.

Madugula M.K.S., Prabhu T.S., Temple M.C. (1983). Ultimate strength of concentrically loaded cold-formed angles, *Canadian Journal of Civil Engineering*, **10**, 60-68.

Može P., Cajot L.-C., Sinur F., Rejec K., Beg D. (2014). Residual stress distribution of large steel equal leg angles, *Engineering Structures*, **71**(July), 35-47.

Popovic D., Hancock G.J., Rasmussen K.J.R. (1999). Axial compression tests of cold-formed angles, *Journal of Structural Engineering* (ASCE), **125**(5), 515-523.

Rasmussen K.J.R. (2006). Design of slender angle section beam-columns by the direct strength method, *Journal of Structural Engineering* (ASCE), 132(2), 204-211.

Schafer B.W. (2008). Review: the direct strength method of cold-formed steel member design, *Journal of Constructional Steel Research*, **64**(7-8), 766-778.

Shi G., Liu Z., Ban H.Y., Zhang Y., Shi Y.J., Wang Y.Q. (2011). Tests and finite element analysis on the local buckling of 420 MPa steel equal angle columns under axial compression, *Steel and Composite Structures*, **12**(1), 31-51.

Silvestre N., Dinis P.B., Camotim D. (2013). Developments on the design of cold-formed steel angles, *Journal of Structural Engineering* (ASCE), 139(5), 680-694.

Wakabayashi M, Nonaka T. (1965). On the buckling strength of angles in transmission towers, *Bulletin of the Disaster Prevention Research Institute*, **15**(2), 1-18.

Young B. (2004). Tests and design of fixed-ended cold-formed steel plain angle columns, *Journal of Structural Engineering* (ASCE), 130(12), 1931-1940.

Young B., Rasmussen K.J.R. (1999). Shift of effective centroid in channel columns, *Journal of Structural Engineering* (ASCE), 125(5), 524-531.

Ziemian R. (ed.) (2010). Guide to Stability Design Criteria for Metal Structures (6th ed.), John Wiley & Sons, Hoboken.

ANNEX A: HOT-ROLLED ANGLE COLUMN EXPERIMENTAL DATA

Table A: HRS angle column geometry, buckling stresses, experimental ultimate stresses, their predictions by the proposed DSM design approach and experimental-to-predicted ratios (dimensions in mm, stresses in MPa)

					Buckling analysis						Proposed DSM Design Approach							
Test	b	t	b/t	L	f_{crft}	f_{cre}	f_{crf}	f_{crt}	f_y	f_u	Δ_f	a	b	c	d	β	f_{nfte}	f_u/f_{nfte}
Wakabayashi & Nonaka (1965)	90	7	12.86	345	22389	5597.1	736.2	727.1	304.0	290.3	1.24	0.42	0.14	0.39	0.84	1.00	297	0.98
	90	7	12.86	708	5316	1329.0	529.7	509.4	304.0	290.3	3.82	0.53	0.15	0.32	0.90	1.00	276	1.05
	90	7	12.86	1062	2363	590.7	493.9	453.5	304.0	281.7	8.18	0.76	0.17	0.12	0.98	1.00	245	1.15
	90	7	12.86	1239	1736	434.0	486.3	432.5	304.0	286.6	11.07	0.87	0.18	0.12	1.00	1.00	227	1.26
Kennedy & Murty (1972)	89	4.8	18.54	1238	1785	446.3	245.3	232.3	345.9	259	5.31	0.61	0.16	0.28	0.94	0.88	177	1.46
	101	7.9	12.78	1231	2325	581.3	522.6	476.5	375.5	312	8.81	0.80	0.18	0.12	0.99	1.00	287	1.09
	76	4.8	15.83	1248	1281	320.3	332.4	298.4	343.8	227	10.22	0.87	0.18	0.12	1.00	0.92	199	1.14
	89	6.4	13.91	1246	1762	440.6	435.9	393.5	394.1	292	9.73	0.85	0.18	0.12	1.00	0.95	258	1.13
Kitipornchai & Lee (1986)	64	4.8	13.33	690	2972	743.0	487.8	456.7	307	282	6.37	0.66	0.17	0.23	0.95	1.00	258	1.09
	102	6.4	15.94	1330	2032	507.9	334.0	312.7	275	228	6.38	0.66	0.17	0.23	0.95	1.00	219	1.04
	102	6.4	15.94	1423	1775	443.7	332.0	307.8	275	217	7.29	0.71	0.17	0.17	0.97	1.00	212	1.02
	64	4.8	13.33	592	4037	1009.3	499.7	475.9	307	273	4.77	0.58	0.16	0.29	0.92	1.00	270	1.01
	76	4.8	15.83	1096	1661	415.3	335.4	309.0	298	215	7.89	0.74	0.17	0.12	0.98	0.94	206	1.04
	76	4.8	15.83	848	2775	693.7	344.3	327.8	298	241	4.78	0.58	0.16	0.29	0.92	1.00	238	1.01
	76	4.8	15.83	997	2007	501.8	338.2	316.0	298	224	6.55	0.67	0.17	0.22	0.96	1.00	227	0.99
Adluri & Madugula (1996)	76	4.8	15.83	915	2383	595.8	341.2	322.3	300	291	5.54	0.62	0.16	0.27	0.94	1.00	234	1.25
	102	7.9	12.91	1215	2435	608.6	513.7	471.3	300	279	8.26	0.76	0.18	0.12	0.98	1.00	244	1.14
	76	4.8	15.83	1213	1356	339.0	333.0	300.8	300	215	9.66	0.84	0.18	0.12	1.00	0.95	197	1.09
Fan (2009)	125	8	15.63	573	16439	4109.8	465.5	460.5	530	393	1.07	0.41	0.14	0.40	0.83	0.98	411	0.96
	125	8	15.63	1877	1532	383.0	343.4	313.2	530	305	8.79	0.79	0.18	0.12	0.99	0.79	200	1.53
	125	10	12.5	384	36604	9150.9	985.5	975.4	525	470	1.02	0.41	0.14	0.40	0.83	1.00	513	0.92
	125	10	12.5	576	16268	4067.1	725.2	712.9	525	458	1.69	0.44	0.14	0.38	0.85	1.00	485	0.94
	160	10	16	736	16325	4081.2	443.0	438.5	555	388	1.02	0.41	0.14	0.40	0.83	0.92	392	0.99
	160	10	16	2311	1656	413.9	328.4	303.0	525	350	7.75	0.73	0.17	0.14	0.98	0.78	196	1.78
	160	12	13.33	491	36681	9170.3	867.0	859.3	530	488	0.89	0.40	0.14	0.41	0.83	1.00	517	0.94
	160	12	13.33	737	16281	4070.2	637.5	628.0	530	477	1.48	0.43	0.14	0.38	0.85	1.00	466	1.02
	160	12	13.33	2169	1880	469.9	475.5	428.1	540	342	9.96	0.86	0.18	0.12	1.00	0.89	283	1.21
Ban, Shi, Shi, Wang (2013)	160	10	16	2559.9	1349	337.4	326.0	295.1	460.7	319	9.50	0.84	0.18	0.12	1.00	0.83	190	1.68
	160	10	16	2558.9	1351	337.6	326.1	295.1	460.7	311	9.49	0.83	0.18	0.12	1.00	0.83	190	1.63
	160	10	16	1593.2	3484	871.0	342.7	329.8	460.7	351	3.77	0.53	0.15	0.32	0.90	0.90	267	1.32
	160	10	16	2561.1	1348	337.1	326.0	295.0	460.7	300	9.51	0.84	0.18	0.12	1.00	0.83	190	1.58
	180	12	15	2865.6	1363	340.7	371.1	331.2	459.4	331	10.74	0.87	0.18	0.12	1.00	0.88	218	1.52
	160	10	16	1920.3	2398	599.5	334.2	316.2	460.7	324	5.39	0.61	0.16	0.27	0.94	0.88	241	1.34
	125	8	15.63	2000.6	1349	337.1	341.9	307.8	442.1	300	9.98	0.86	0.18	0.12	1.00	0.85	201	1.49
	128	8	16	1249.2	3627	906.7	343.8	331.3	442.1	350	3.63	0.52	0.15	0.32	0.90	0.92	270	1.30
	125	8	15.63	2000.7	1348	337.1	341.9	307.7	442.1	304	9.98	0.86	0.18	0.12	1.00	0.85	201	1.51
	160	10	16	1920.9	2397	599.2	334.2	316.2	460.7	322	5.39	0.61	0.16	0.27	0.94	0.88	241	1.33
	180	12	15	2146.8	2428	607.1	380.6	357.4	459.4	357	6.08	0.65	0.16	0.24	0.95	0.92	267	1.34
	180	12	15	2863.8	1365	341.2	371.1	331.3	459.4	321	10.73	0.87	0.18	0.12	1.00	0.88	218	1.47
	180	12	15	2142.8	2438	609.4	380.6	357.6	459.4	349	6.06	0.64	0.16	0.24	0.95	0.92	268	1.30
	160	10	16	1920.9	2397	599.2	334.2	316.2	460.7	313	5.39	0.61	0.16	0.27	0.94	0.88	241	1.30
	180	12	15	2862.6	1366	341.5	371.1	331.3	459.4	314	10.72	0.87	0.18	0.12	1.00	0.88	218	1.44
	160	10	16	1600.4	3453	863.2	342.5	329.4	460.7	328	3.81	0.53	0.15	0.32	0.90	0.90	266	1.23
	180	12	15	2148	2426	606.4	380.5	357.4	459.4	346	6.09	0.65	0.16	0.24	0.95	0.92	267	1.30
	125	8	15.63	1500.6	2397	599.2	350.5	330.6	442.1	321	5.66	0.62	0.16	0.26	0.94	0.92	251	1.28
	140	10	14	1389.9	3505	876.2	447.9	425.8	449.1	387	4.93	0.59	0.16	0.29	0.93	1.00	329	1.18
	180	12	15	1789.3	3496	873.9	390.0	373.3	459.4	360	4.29	0.56	0.16	0.31	0.91	0.96	300	1.20
	160	10	16	1611.7	3404	851.1	342.1	328.9	460.7	318	3.86	0.53	0.15	0.32	0.90	0.90	265	1.20
	160	10	16	1274.2	5447	1361.7	358.1	349.1	460.7	339	2.50	0.47	0.15	0.35	0.87	0.91	294	1.15

					Buckling analysis						Proposed DSM Design Approach							
Test	b	t	b/t	L	f_{crft}	f_{cre}	f_{crf}	f_{crt}	f_y	f_u	Δ_f	a	b	c	d	β	f_{nfte}	f_u/f_{nfte}
Ban, Shi, Shi, Wang (2013)	125	8	15.63	1499.4	2401	600.2	350.5	330.7	442.1	314	5.65	0.62	0.16	0.26	0.94	0.92	251	1.25
	140	10	14	1390.5	3502	875.4	447.8	425.7	449.1	377	4.93	0.59	0.16	0.29	0.93	1.00	329	1.15
	160	10	16	1278.6	5409	1352.3	357.8	348.8	460.7	338	2.52	0.47	0.15	0.35	0.87	0.91	294	1.15
	180	12	15	1790.1	3493	873.2	390.0	373.3	459.4	352	4.29	0.56	0.16	0.31	0.91	0.96	300	1.17
	140	10	14	1389.4	3507	876.8	447.9	425.8	449.1	374	4.93	0.59	0.16	0.29	0.93	1.00	329	1.14
	180	12	15	1791.7	3486	871.6	390.0	373.2	459.4	344	4.30	0.56	0.16	0.31	0.91	0.96	300	1.15
	125	8	15.63	1500.4	2398	599.4	350.5	330.6	442.1	305	5.66	0.62	0.16	0.26	0.94	0.92	251	1.21
	180	12	15	1432.7	5453	1363.1	407.4	395.8	459.4	362	2.85	0.49	0.15	0.34	0.88	0.98	332	1.09
	125	8	15.63	1250.8	3450	862.5	359.1	344.7	442.1	314	4.00	0.54	0.15	0.32	0.91	0.94	279	1.13
	160	10	16	1275.3	5437	1359.3	358.0	349.0	460.7	322	2.51	0.47	0.15	0.35	0.87	0.91	294	1.10
	160	10	16	959.5	9605	2401.4	390.5	384.5	460.7	356	1.54	0.43	0.14	0.38	0.85	0.96	336	1.06
	125	8	15.63	1250.7	3450	862.6	359.1	344.7	442.1	311	4.00	0.54	0.15	0.32	0.91	0.94	279	1.12
	125	8	15.63	1998.4	1352	337.9	341.9	307.9	442.1	265	9.96	0.86	0.18	0.12	1.00	0.85	201	1.32
	200	14	14.29	1990.5	3487	871.9	429.9	409.5	448.8	347	4.75	0.58	0.16	0.29	0.92	1.00	323	1.08
	180	12	15	1432.1	5457	1364.3	407.5	395.9	459.4	351	2.85	0.49	0.15	0.34	0.88	0.98	332	1.06
	140	10	14	834.2	9729	2432.3	511.4	501.2	449.1	408	2.00	0.45	0.14	0.37	0.86	1.00	381	1.07
	125	8	15.63	1000.2	5395	1348.8	375.0	365.1	442.1	324	2.65	0.48	0.15	0.35	0.88	0.96	307	1.05
	180	12	15	1432.3	5456	1363.9	407.5	395.9	459.4	345	2.85	0.49	0.15	0.34	0.88	0.98	332	1.04
	160	10	16	957.8	9640	2409.9	390.8	384.8	460.7	344	1.54	0.43	0.14	0.38	0.85	0.96	337	1.02
	125	10	12.5	749.3	9613	2403.3	640.0	623.7	442.1	355	2.54	0.47	0.15	0.35	0.87	1.00	409	0.87
	180	12	15	1071.3	9752	2438.0	445.7	437.9	459.4	383	1.73	0.44	0.14	0.38	0.85	1.00	368	1.04
	160	10	16	956.8	9660	2414.9	391.0	385.0	460.7	341	1.53	0.43	0.14	0.38	0.85	0.96	337	1.01
	125	8	15.63	999.6	5402	1350.4	375.1	365.2	442.1	317	2.65	0.48	0.15	0.35	0.88	0.96	307	1.03
	200	14	14.29	1189.8	9761	2440.2	491.4	482.0	448.8	389	1.91	0.45	0.14	0.37	0.86	1.00	376	1.03
	140	10	14	833.9	9736	2434.1	511.4	501.2	449.1	393	1.99	0.45	0.14	0.37	0.86	1.00	381	1.03
	140	10	14	833.7	9741	2435.3	511.5	501.3	449.1	393	1.99	0.45	0.14	0.37	0.86	1.00	381	1.03
	180	12	15	1075.1	9683	2420.8	445.0	437.3	459.4	374	1.74	0.44	0.14	0.38	0.85	1.00	368	1.02
	200	14	14.29	1990.3	3488	872.0	430.0	409.5	448.8	333	4.75	0.58	0.16	0.29	0.92	1.00	323	1.03
	180	12	15	1073.7	9708	2427.1	445.3	437.5	459.4	372	1.74	0.44	0.14	0.38	0.85	1.00	368	1.01
	125	8	15.63	998.6	5413	1353.1	375.2	365.3	442.1	306	2.64	0.48	0.15	0.35	0.88	0.96	308	0.99
	200	14	14.29	1194.7	9681	2420.2	490.6	481.2	448.8	376	1.92	0.45	0.14	0.37	0.86	1.00	375	1.00
	200	14	14.29	1194.9	9678	2419.4	490.6	481.2	448.8	375	1.92	0.45	0.14	0.37	0.86	1.00	375	1.00
	125	8	15.63	750.3	9588	2396.9	409.4	402.8	442.1	335	1.62	0.43	0.14	0.38	0.85	1.00	349	0.96
	200	14	14.29	1989.7	3490	872.6	430.0	409.6	448.8	320	4.75	0.58	0.16	0.29	0.92	1.00	323	0.99
	125	8	15.63	749.2	9616	2404.0	409.6	403.0	442.1	327	1.61	0.43	0.14	0.38	0.85	1.00	349	0.94
																Mean		1.16
																Sd. Dev.		0.19
																Max		1.78
																Min		0.87

ANNEX B: HOT-ROLLED ANGLE COLUMN NUMERICAL DATA

Table B: HRS angle column geometry, buckling stresses, numerical ultimate stresses, their predictions by the proposed DSM design approach and numerical-to-predicted ratios (dimensions in mm, stresses in MPa)

				Buckling analysis						Proposed DSM Design Approach							
b	t	b/t	L	f_{crft}	f_{cre}	f_{crf}	f_{crt}	f_y	f_u	Δ_f	a	b	c	d	β	f_{nfte}	f_u/f_{nfte}
50	4.55	11	582	2550	637.4	709.7	631.6	150	130	10.99	0.87	0.18	0.12	1.00	1.00	136	0.96
50	4.55	11	582	2550	637.4	709.7	631.6	300	238	10.99	0.87	0.18	0.12	1.00	1.00	246	0.97
50	4.55	11	582	2550	637.4	709.7	631.6	500	355	10.99	0.87	0.18	0.12	1.00	1.00	360	0.99
50	4.55	11	582	2550	637.4	709.7	631.6	700	435	10.99	0.87	0.18	0.12	1.00	0.94	417	1.04
50	4.55	11	436.5	4533	1133.1	742.4	695.2	150	137	3.33	0.66	0.17	0.23	0.95	1.00	142	0.97
50	4.55	11	436.5	4533	1133.1	742.4	695.2	300	262	3.33	0.66	0.17	0.23	0.95	1.00	269	0.98
50	4.55	11	436.5	4533	1133.1	742.4	695.2	500	409	3.33	0.66	0.17	0.23	0.95	1.00	416	0.98
50	4.55	11	436.5	4533	1133.1	742.4	695.2	700	521	3.33	0.66	0.17	0.23	0.95	1.00	513	1.02
50	4.55	11	291	10198	2549.5	836.1	809.9	150	143	3.13	0.50	0.15	0.34	0.89	1.00	146	0.98
50	4.55	11	291	10198	2549.5	836.1	809.9	300	280	3.13	0.50	0.15	0.34	0.89	1.00	286	0.98
50	4.55	11	291	10198	2549.5	836.1	809.9	500	449	3.13	0.50	0.15	0.34	0.89	1.00	461	0.97
50	4.55	11	291	10198	2549.5	836.1	809.9	700	580	3.13	0.50	0.15	0.34	0.89	1.00	590	0.98
50	4.55	11	145.5	40793	10198.2	1341.8	1325.1	150	146	1.24	0.42	0.14	0.39	0.84	1.00	149	0.98
50	4.55	11	145.5	40793	10198.2	1341.8	1325.1	300	291	1.24	0.42	0.14	0.39	0.84	1.00	296	0.98
50	4.55	11	145.5	40793	10198.2	1341.8	1325.1	500	475	1.24	0.42	0.14	0.39	0.84	1.00	490	0.97
50	4.55	11	145.5	40793	10198.2	1341.8	1325.1	700	638	1.24	0.42	0.14	0.39	0.84	1.00	680	0.94
50	3.33	15	806	1329	332.3	370.8	329.9	150	116	11.02	0.87	0.18	0.12	1.00	1.00	124	0.93
50	3.33	15	806	1329	332.3	370.8	329.9	300	194	11.02	0.87	0.18	0.12	1.00	1.00	206	0.94
50	3.33	15	806	1329	332.3	370.8	329.9	500	245	11.02	0.87	0.18	0.12	1.00	0.87	217	1.13
50	3.33	15	806	1329	332.3	370.8	329.9	700	247	11.02	0.87	0.18	0.12	1.00	0.83	213	1.16
50	3.33	15	604.5	2363	590.8	380.0	356.3	150	128	6.24	0.65	0.17	0.24	0.95	1.00	135	0.95
50	3.33	15	604.5	2363	590.8	380.0	356.3	300	233	6.24	0.65	0.17	0.24	0.95	1.00	243	0.96
50	3.33	15	604.5	2363	590.8	380.0	356.3	500	296	6.24	0.65	0.17	0.24	0.95	0.89	262	1.13
50	3.33	15	604.5	2363	590.8	380.0	356.3	700	296	6.24	0.65	0.17	0.24	0.95	0.79	254	1.16
50	3.33	15	403	5317	1329.3	406.2	394.4	150	139	2.92	0.49	0.15	0.34	0.88	1.00	143	0.97
50	3.33	15	403	5317	1329.3	406.2	394.4	300	262	2.92	0.49	0.15	0.34	0.88	1.00	269	0.97
50	3.33	15	403	5317	1329.3	406.2	394.4	500	335	2.92	0.49	0.15	0.34	0.88	0.93	329	1.02
50	3.33	15	403	5317	1329.3	406.2	394.4	700	343	2.92	0.49	0.15	0.34	0.88	0.78	324	1.06
50	3.33	15	201.5	21270	5317.4	548.0	542.7	150	145	0.97	0.41	0.14	0.40	0.83	1.00	148	0.98
50	3.33	15	201.5	21270	5317.4	548.0	542.7	300	280	0.97	0.41	0.14	0.40	0.83	1.00	293	0.96
50	3.33	15	201.5	21270	5317.4	548.0	542.7	500	398	0.97	0.41	0.14	0.40	0.83	1.00	431	0.92
50	3.33	15	201.5	21270	5317.4	548.0	542.7	700	451	0.97	0.41	0.14	0.40	0.83	0.91	486	0.93
50	2.5	20	1080	740	185.1	205.6	183.1	150	96.1	10.97	0.87	0.18	0.12	1.00	1.00	107	0.90
50	2.5	20	1080	740	185.1	205.6	183.1	300	133	10.97	0.87	0.18	0.12	1.00	0.85	119	1.11
50	2.5	20	1080	740	185.1	205.6	183.1	500	133	10.97	0.87	0.18	0.12	1.00	0.82	118	1.13
50	2.5	20	1080	740	185.1	205.6	183.1	700	131	10.97	0.87	0.18	0.12	1.00	0.82	118	1.11
50	2.5	20	813	1307	326.6	208.5	195.5	150	115	6.19	0.65	0.16	0.24	0.95	1.00	124	0.93
50	2.5	20	813	1307	326.6	208.5	195.5	300	163	6.19	0.65	0.16	0.24	0.95	0.86	143	1.14
50	2.5	20	813	1307	326.6	208.5	195.5	500	161	6.19	0.65	0.16	0.24	0.95	0.73	138	1.17
50	2.5	20	813	1307	326.6	208.5	195.5	700	158	6.19	0.65	0.16	0.24	0.95	0.70	136	1.16
50	2.5	20	542	2940	734.9	216.6	210.5	150	131	2.81	0.49	0.15	0.34	0.88	1.00	138	0.95
50	2.5	20	542	2940	734.9	216.6	210.5	300	184	2.81	0.49	0.15	0.34	0.88	0.87	175	1.05
50	2.5	20	542	2940	734.9	216.6	210.5	500	183	2.81	0.49	0.15	0.34	0.88	0.69	173	1.06
50	2.5	20	542	2940	734.9	216.6	210.5	700	180	2.81	0.49	0.15	0.34	0.88	0.60	172	1.04
50	2.5	20	271	11759	2939.7	260.7	258.5	150	141	0.84	0.40	0.14	0.41	0.83	1.00	147	0.96
50	2.5	20	271	11759	2939.7	260.7	258.5	300	216	0.84	0.40	0.14	0.41	0.83	0.98	233	0.93
50	2.5	20	271	11759	2939.7	260.7	258.5	500	233	0.84	0.40	0.14	0.41	0.83	0.72	235	0.99
50	2.5	20	271	11759	2939.7	260.7	258.5	700	236	0.84	0.40	0.14	0.41	0.83	0.60	240	0.98

				Buckling analysis						Proposed DSM Design Approach							
b	t	b/t	L	f_{crft}	f_{cre}	f_{crf}	f_{crt}	f_y	f_u	Δ_f	a	b	c	d	β	f_{nfte}	f_u/f_{nfte}
70	3.33	11	815	2548	637.1	709.6	631.6	150	130	11.00	0.87	0.18	0.12	1.00	1.00	136	0.96
70	3.33	11	815	2548	637.1	709.6	631.6	300	238	11.00	0.87	0.18	0.12	1.00	1.00	246	0.97
70	3.33	11	815	2548	637.1	709.6	631.6	500	355	11.00	0.87	0.18	0.12	1.00	1.00	360	0.99
70	3.33	11	815	2548	637.1	709.6	631.6	700	434	11.00	0.87	0.18	0.12	1.00	0.94	416	1.04
70	3.33	11	611.25	4530	1132.6	742.4	695.1	150	137	3.33	0.66	0.17	0.23	0.95	1.00	142	0.97
70	3.33	11	611.25	4530	1132.6	742.4	695.1	300	262	3.33	0.66	0.17	0.23	0.95	1.00	269	0.98
70	3.33	11	611.25	4530	1132.6	742.4	695.1	500	409	3.33	0.66	0.17	0.23	0.95	1.00	416	0.98
70	3.33	11	611.25	4530	1132.6	742.4	695.1	700	521	3.33	0.66	0.17	0.23	0.95	1.00	513	1.02
70	3.33	11	407.5	10193	2548.3	836.0	809.8	150	143	3.13	0.50	0.15	0.34	0.89	1.00	146	0.98
70	3.33	11	407.5	10193	2548.3	836.0	809.8	300	280	3.13	0.50	0.15	0.34	0.89	1.00	286	0.98
70	3.33	11	407.5	10193	2548.3	836.0	809.8	500	449	3.13	0.50	0.15	0.34	0.89	1.00	461	0.97
70	3.33	11	407.5	10193	2548.3	836.0	809.8	700	580	3.13	0.50	0.15	0.34	0.89	1.00	590	0.98
70	3.33	11	203.75	40773	10193.2	1341.4	1324.8	150	146	1.24	0.42	0.14	0.39	0.84	1.00	149	0.98
70	3.33	11	203.75	40773	10193.2	1341.4	1324.8	300	291	1.24	0.42	0.14	0.39	0.84	1.00	296	0.98
70	3.33	11	203.75	40773	10193.2	1341.4	1324.8	500	475	1.24	0.42	0.14	0.39	0.84	1.00	490	0.97
70	3.33	11	203.75	40773	10193.2	1341.4	1324.8	700	638	1.24	0.42	0.14	0.39	0.84	1.00	680	0.94
70	4.67	15	1130	1326	331.4	370.8	329.8	150	116	11.05	0.87	0.18	0.12	1.00	1.00	124	0.93
70	4.67	15	1130	1326	331.4	370.8	329.8	300	194	11.05	0.87	0.18	0.12	1.00	1.00	205	0.94
70	4.67	15	1130	1326	331.4	370.8	329.8	500	245	11.05	0.87	0.18	0.12	1.00	0.87	217	1.13
70	4.67	15	1130	1326	331.4	370.8	329.8	700	247	11.05	0.87	0.18	0.12	1.00	0.83	213	1.16
70	4.67	15	847.5	2357	589.1	379.9	356.1	150	128	6.26	0.65	0.17	0.23	0.95	1.00	135	0.95
70	4.67	15	847.5	2357	589.1	379.9	356.1	300	233	6.26	0.65	0.17	0.23	0.95	1.00	242	0.96
70	4.67	15	847.5	2357	589.1	379.9	356.1	500	296	6.26	0.65	0.17	0.23	0.95	0.89	261	1.13
70	4.67	15	847.5	2357	589.1	379.9	356.1	700	296	6.26	0.65	0.17	0.23	0.95	0.79	254	1.17
70	4.67	15	565	5302	1325.6	406.1	394.2	150	139	2.92	0.49	0.15	0.34	0.88	1.00	143	0.97
70	4.67	15	565	5302	1325.6	406.1	394.2	300	262	2.92	0.49	0.15	0.34	0.88	1.00	269	0.98
70	4.67	15	565	5302	1325.6	406.1	394.2	500	335	2.92	0.49	0.15	0.34	0.88	0.93	328	1.02
70	4.67	15	565	5302	1325.6	406.1	394.2	700	343	2.92	0.49	0.15	0.34	0.88	0.78	324	1.06
70	4.67	15	282.5	21209	5302.3	547.5	542.2	150	145	0.97	0.41	0.14	0.40	0.83	1.00	148	0.98
70	4.67	15	282.5	21209	5302.3	547.5	542.2	300	280	0.97	0.41	0.14	0.40	0.83	1.00	293	0.96
70	4.67	15	282.5	21209	5302.3	547.5	542.2	500	398	0.97	0.41	0.14	0.40	0.83	1.00	431	0.92
70	4.67	15	282.5	21209	5302.3	547.5	542.2	700	451	0.97	0.41	0.14	0.40	0.83	0.91	486	0.93
70	3.5	20	1514	738	184.6	205.6	183.0	150	96	11.00	0.87	0.18	0.12	1.00	1.00	107	0.90
70	3.5	20	1514	738	184.6	205.6	183.0	300	133	11.00	0.87	0.18	0.12	1.00	0.85	119	1.11
70	3.5	20	1514	738	184.6	205.6	183.0	500	132	11.00	0.87	0.18	0.12	1.00	0.82	118	1.12
70	3.5	20	1514	738	184.6	205.6	183.0	700	131	11.00	0.87	0.18	0.12	1.00	0.82	118	1.11
70	3.5	20	1135.5	1313	328.2	208.5	195.6	150	115	6.16	0.65	0.16	0.24	0.95	1.00	124	0.93
70	3.5	20	1135.5	1313	328.2	208.5	195.6	300	162	6.16	0.65	0.16	0.24	0.95	0.86	143	1.13
70	3.5	20	1135.5	1313	328.2	208.5	195.6	500	161	6.16	0.65	0.16	0.24	0.95	0.73	138	1.17
70	3.5	20	1135.5	1313	328.2	208.5	195.6	700	158	6.16	0.65	0.16	0.24	0.95	0.70	136	1.16
70	3.5	20	757	2954	738.4	216.7	210.6	150	131	2.80	0.48	0.15	0.35	0.88	1.00	138	0.95
70	3.5	20	757	2954	738.4	216.7	210.6	300	184	2.80	0.48	0.15	0.35	0.88	0.88	175	1.05
70	3.5	20	757	2954	738.4	216.7	210.6	500	183	2.80	0.48	0.15	0.35	0.88	0.68	173	1.06
70	3.5	20	757	2954	738.4	216.7	210.6	700	180	2.80	0.48	0.15	0.35	0.88	0.60	172	1.04
70	3.5	20	378.5	11815	2953.7	261.0	258.8	150	141	0.83	0.40	0.14	0.41	0.83	1.00	147	0.96
70	3.5	20	378.5	11815	2953.7	261.0	258.8	300	216	0.83	0.40	0.14	0.41	0.83	0.98	233	0.93
70	3.5	20	378.5	11815	2953.7	261.0	258.8	500	233	0.83	0.40	0.14	0.41	0.83	0.72	235	0.99
70	3.5	20	378.5	11815	2953.7	261.0	258.8	700	237	0.83	0.40	0.14	0.41	0.83	0.60	240	0.99
90	8.18	11	1050	2538	634.5	709.5	631.1	150	130	11.04	0.87	0.18	0.12	1.00	1.00	136	0.96
90	8.18	11	1050	2538	634.5	709.5	631.1	300	238	11.04	0.87	0.18	0.12	1.00	1.00	246	0.97
90	8.18	11	1050	2538	634.5	709.5	631.1	500	354	11.04	0.87	0.18	0.12	1.00	1.00	360	0.98
90	8.18	11	1050	2538	634.5	709.5	631.1	700	434	11.04	0.87	0.18	0.12	1.00	0.94	416	1.04

				Buckling analysis						Proposed DSM Design Approach							
b	t	b/t	L	f_{crft}	f_{cre}	f_{crf}	f_{crt}	f_y	f_u	Δ_f	a	b	c	d	β	f_{nfte}	f_u/f_{nfte}
90	8.18	11	787.5	4512	1128.0	742.1	694.7	150	137	6.39	0.66	0.17	0.23	0.95	1.00	142	0.97
90	8.18	11	787.5	4512	1128.0	742.1	694.7	300	262	6.39	0.66	0.17	0.23	0.95	1.00	268	0.98
90	8.18	11	787.5	4512	1128.0	742.1	694.7	500	408	6.39	0.66	0.17	0.23	0.95	1.00	415	0.98
90	8.18	11	787.5	4512	1128.0	742.1	694.7	700	520	6.39	0.66	0.17	0.23	0.95	1.00	513	1.01
90	8.18	11	525	10152	2537.9	835.3	809.0	150	143	3.15	0.50	0.15	0.34	0.89	1.00	146	0.98
90	8.18	11	525	10152	2537.9	835.3	809.0	300	280	3.15	0.50	0.15	0.34	0.89	1.00	286	0.98
90	8.18	11	525	10152	2537.9	835.3	809.0	500	449	3.15	0.50	0.15	0.34	0.89	1.00	460	0.98
90	8.18	11	525	10152	2537.9	835.3	809.0	700	579	3.15	0.50	0.15	0.34	0.89	1.00	589	0.98
90	8.18	11	262.5	40606	10151.6	1338.7	1322.0	150	146	1.25	0.42	0.14	0.39	0.84	1.00	149	0.98
90	8.18	11	262.5	40606	10151.6	1338.7	1322.0	300	291	1.25	0.42	0.14	0.39	0.84	1.00	296	0.98
90	8.18	11	262.5	40606	10151.6	1338.7	1322.0	500	475	1.25	0.42	0.14	0.39	0.84	1.00	490	0.97
90	8.18	11	262.5	40606	10151.6	1338.7	1322.0	700	638	1.25	0.42	0.14	0.39	0.84	1.00	680	0.94
90	6	15	1450	1331	332.7	370.8	330.0	150	116	11.00	0.87	0.18	0.12	1.00	1.00	124	0.93
90	6	15	1450	1331	332.7	370.8	330.0	300	194	11.00	0.87	0.18	0.12	1.00	1.00	206	0.94
90	6	15	1450	1331	332.7	370.8	330.0	500	245	11.00	0.87	0.18	0.12	1.00	0.87	217	1.13
90	6	15	1450	1331	332.7	370.8	330.0	700	247	11.00	0.87	0.18	0.12	1.00	0.83	213	1.16
90	6	15	1087.5	2366	591.5	380.0	356.3	150	128	6.23	0.65	0.17	0.24	0.95	1.00	135	0.95
90	6	15	1087.5	2366	591.5	380.0	356.3	300	233	6.23	0.65	0.17	0.24	0.95	1.00	243	0.96
90	6	15	1087.5	2366	591.5	380.0	356.3	500	298	6.23	0.65	0.17	0.24	0.95	0.89	262	1.14
90	6	15	1087.5	2366	591.5	380.0	356.3	700	297	6.23	0.65	0.17	0.24	0.95	0.79	255	1.17
90	6	15	725	5323	1330.8	406.3	394.5	150	139	2.91	0.49	0.15	0.34	0.88	1.00	143	0.97
90	6	15	725	5323	1330.8	406.3	394.5	300	262	2.91	0.49	0.15	0.34	0.88	1.00	269	0.97
90	6	15	725	5323	1330.8	406.3	394.5	500	335	2.91	0.49	0.15	0.34	0.88	0.93	329	1.02
90	6	15	725	5323	1330.8	406.3	394.5	700	343	2.91	0.49	0.15	0.34	0.88	0.78	324	1.06
90	6	15	362.5	21293	5323.2	548.2	542.9	150	145	0.97	0.41	0.14	0.40	0.83	1.00	148	0.98
90	6	15	362.5	21293	5323.2	548.2	542.9	300	280	0.97	0.41	0.14	0.40	0.83	1.00	293	0.96
90	6	15	362.5	21293	5323.2	548.2	542.9	500	398	0.97	0.41	0.14	0.40	0.83	1.00	431	0.92
90	6	15	362.5	21293	5323.2	548.2	542.9	700	451	0.97	0.41	0.14	0.40	0.83	0.91	487	0.93
90	4.5	20	1945	740	184.9	205.6	183.0	150	96.1	10.98	0.87	0.18	0.12	1.00	1.00	107	0.90
90	4.5	20	1945	740	184.9	205.6	183.0	300	133	10.98	0.87	0.18	0.12	1.00	0.85	119	1.11
90	4.5	20	1945	740	184.9	205.6	183.0	500	133	10.98	0.87	0.18	0.12	1.00	0.82	118	1.13
90	4.5	20	1945	740	184.9	205.6	183.0	700	131	10.98	0.87	0.18	0.12	1.00	0.82	118	1.11
90	4.5	20	1462.5	1308	327.0	208.5	195.6	150	115	6.18	0.65	0.16	0.24	0.95	1.00	124	0.93
90	4.5	20	1462.5	1308	327.0	208.5	195.6	300	163	6.18	0.65	0.16	0.24	0.95	0.86	143	1.14
90	4.5	20	1462.5	1308	327.0	208.5	195.6	500	161	6.18	0.65	0.16	0.24	0.95	0.73	138	1.17
90	4.5	20	1462.5	1308	327.0	208.5	195.6	700	158	6.18	0.65	0.16	0.24	0.95	0.70	136	1.16
90	4.5	20	975	2943	735.8	216.6	210.6	150	131	2.81	0.49	0.15	0.35	0.88	1.00	138	0.95
90	4.5	20	975	2943	735.8	216.6	210.6	300	184	2.81	0.49	0.15	0.35	0.88	0.87	175	1.05
90	4.5	20	975	2943	735.8	216.6	210.6	500	183	2.81	0.49	0.15	0.35	0.88	0.69	173	1.06
90	4.5	20	975	2943	735.8	216.6	210.6	700	180	2.81	0.49	0.15	0.35	0.88	0.60	172	1.04
90	4.5	20	487.5	11773	2943.4	260.8	258.6	150	141	0.84	0.40	0.14	0.41	0.83	1.00	147	0.96
90	4.5	20	487.5	11773	2943.4	260.8	258.6	300	216	0.84	0.40	0.14	0.41	0.83	0.98	233	0.93
90	4.5	20	487.5	11773	2943.4	260.8	258.6	500	233	0.84	0.40	0.14	0.41	0.83	0.72	235	0.99
90	4.5	20	487.5	11773	2943.4	260.8	258.6	700	236	0.84	0.40	0.14	0.41	0.83	0.60	240	0.98
																Mean	1.01
																Sd. Dev.	0.08
																Max	1.17
																Min	0.90

ANNEX C: COLD-FORMED ANGLE COLUMN NUMERICAL DATA

Table C: CFS angle column geometry, buckling stresses, numerical ultimate stresses, their predictions by the proposed DSM design approach and numerical-to-predicted ratios (dimensions in mm, stresses in MPa)

				Buckling analysis						Proposed DSM Design Approach							
b	t	b/t	L	f_{crft}	f_{cre}	f_{crf}	f_{crt}	f_y	f_u	Δ_f	a	b	c	d	β	f_{nfte}	f_u/f_{nfte}
50	2	25	1350	474	118.5	130.7	116.5	300	88	10.89	0.87	0.18	0.12	1.00	0.82	75	1.17
50	2	25	1350	474	118.5	130.7	116.5	500	88	10.89	0.87	0.18	0.12	1.00	0.82	75	1.17
50	2	25	1350	474	118.5	130.7	116.5	150	84.4	10.89	0.87	0.18	0.12	1.00	0.90	77	1.09
50	2	25	1350	474	118.5	130.7	116.5	700	88	10.89	0.87	0.18	0.12	1.00	0.82	75	1.17
50	2	25	1020	830	207.5	131.9	123.8	300	108	6.17	0.65	0.16	0.24	0.95	0.74	87	1.23
50	2	25	1020	830	207.5	131.9	123.8	500	108	6.17	0.65	0.16	0.24	0.95	0.70	86	1.25
50	2	25	1020	830	207.5	131.9	123.8	150	105	6.17	0.65	0.16	0.24	0.95	0.95	93	1.13
50	2	25	1020	830	207.5	131.9	123.8	700	108	6.17	0.65	0.16	0.24	0.95	0.70	86	1.25
50	2	25	680	1868	466.9	135.2	131.5	300	121	2.76	0.48	0.15	0.35	0.88	0.70	108	1.12
50	2	25	680	1868	466.9	135.2	131.5	500	121	2.76	0.48	0.15	0.35	0.88	0.57	108	1.12
50	2	25	680	1868	466.9	135.2	131.5	150	117	2.76	0.48	0.15	0.35	0.88	0.99	111	1.06
50	2	25	680	1868	466.9	135.2	131.5	700	121	2.76	0.48	0.15	0.35	0.88	0.53	108	1.12
50	2	25	340	7471	1867.6	153.1	152.0	300	145	0.77	0.40	0.14	0.41	0.83	0.71	139	1.05
50	2	25	340	7471	1867.6	153.1	152.0	500	149	0.77	0.40	0.14	0.41	0.83	0.55	144	1.04
50	2	25	340	7471	1867.6	153.1	152.0	150	128	0.77	0.40	0.14	0.41	0.83	1.00	126	1.01
50	2	25	340	7471	1867.6	153.1	152.0	700	152	0.77	0.40	0.14	0.41	0.83	0.47	148	1.03
50	1.25	40	2175	183	45.6	50.7	45.1	300	31.2	10.97	0.87	0.18	0.12	1.00	0.82	29	1.07
50	1.25	40	2175	183	45.6	50.7	45.1	500	31.2	10.97	0.87	0.18	0.12	1.00	0.82	29	1.07
50	1.25	40	2175	183	45.6	50.7	45.1	150	31.2	10.97	0.87	0.18	0.12	1.00	0.82	29	1.07
50	1.25	40	2175	183	45.6	50.7	45.1	700	31.2	10.97	0.87	0.18	0.12	1.00	0.82	29	1.07
50	1.25	40	1635	323	80.8	50.9	47.8	300	42	6.11	0.65	0.16	0.24	0.95	0.70	33	1.26
50	1.25	40	1635	323	80.8	50.9	47.8	500	42	6.11	0.65	0.16	0.24	0.95	0.70	33	1.26
50	1.25	40	1635	323	80.8	50.9	47.8	150	42	6.11	0.65	0.16	0.24	0.95	0.71	33	1.25
50	1.25	40	1635	323	80.8	50.9	47.8	700	42	6.11	0.65	0.16	0.24	0.95	0.70	33	1.26
50	1.25	40	1090	727	181.7	51.4	50.0	300	45.4	2.70	0.48	0.15	0.35	0.88	0.51	41	1.10
50	1.25	40	1090	727	181.7	51.4	50.0	500	45.4	2.70	0.48	0.15	0.35	0.88	0.49	41	1.10
50	1.25	40	1090	727	181.7	51.4	50.0	150	45.4	2.70	0.48	0.15	0.35	0.88	0.62	41	1.10
50	1.25	40	1090	727	181.7	51.4	50.0	700	45.4	2.70	0.48	0.15	0.35	0.88	0.49	41	1.10
50	1.25	40	545	2907	726.9	54.1	53.7	300	54.5	0.70	0.40	0.14	0.42	0.82	0.43	54	1.02
50	1.25	40	545	2907	726.9	54.1	53.7	500	56.3	0.70	0.40	0.14	0.42	0.82	0.35	56	1.00
50	1.25	40	545	2907	726.9	54.1	53.7	150	52.4	0.70	0.40	0.14	0.42	0.82	0.59	50	1.04
50	1.25	40	545	2907	726.9	54.1	53.7	700	56.9	0.70	0.40	0.14	0.42	0.82	0.32	58	0.98
50	0.86	58.33	3183	85	21.3	23.8	21.2	300	13.7	11.02	0.87	0.18	0.12	1.00	0.82	14	1.00
50	0.86	58.33	3183	85	21.3	23.8	21.2	500	13.7	11.02	0.87	0.18	0.12	1.00	0.82	14	1.00
50	0.86	58.33	3183	85	21.3	23.8	21.2	150	13.7	11.02	0.87	0.18	0.12	1.00	0.82	14	1.00
50	0.86	58.33	3183	85	21.3	23.8	21.2	700	13.7	11.02	0.87	0.18	0.12	1.00	0.82	14	1.00
50	0.86	58.33	2391	151	37.8	23.8	22.4	300	16.9	6.12	0.65	0.16	0.24	0.95	0.70	16	1.08
50	0.86	58.33	2391	151	37.8	23.8	22.4	500	16.9	6.12	0.65	0.16	0.24	0.95	0.70	16	1.08
50	0.86	58.33	2391	151	37.8	23.8	22.4	150	16.9	6.12	0.65	0.16	0.24	0.95	0.70	16	1.08
50	0.86	58.33	2391	151	37.8	23.8	22.4	700	16.9	6.12	0.65	0.16	0.24	0.95	0.70	16	1.08
50	0.86	58.33	1594	340	85.0	23.9	23.3	300	20.2	2.68	0.48	0.15	0.35	0.88	0.49	19	1.05
50	0.86	58.33	1594	340	85.0	23.9	23.3	500	20.2	2.68	0.48	0.15	0.35	0.88	0.49	19	1.05
50	0.86	58.33	1594	340	85.0	23.9	23.3	150	20.2	2.68	0.48	0.15	0.35	0.88	0.50	19	1.05
50	0.86	58.33	1594	340	85.0	23.9	23.3	700	20.2	2.68	0.48	0.15	0.35	0.88	0.49	19	1.05
50	0.86	58.33	797	1360	339.9	24.5	24.4	300	25.4	0.68	0.40	0.14	0.42	0.82	0.32	26	0.96
50	0.86	58.33	797	1360	339.9	24.5	24.4	500	25.4	0.68	0.40	0.14	0.42	0.82	0.28	27	0.93
50	0.86	58.33	797	1360	339.9	24.5	24.4	150	24.6	0.68	0.40	0.14	0.42	0.82	0.41	25	1.00
50	0.86	58.33	797	1360	339.9	24.5	24.4	700	25.4	0.68	0.40	0.14	0.42	0.82	0.27	28	0.91

				Buckling analysis						Proposed DSM Design Approach							
b	t	b/t	L	f_{crft}	f_{cre}	f_{crf}	f_{crt}	f_y	f_u	Δ_f	a	b	c	d	β	f_{nfte}	f_u/f_{nfte}
70	2.8	25	1895	471	117.8	130.7	116.4	150	80.5	10.95	0.87	0.18	0.12	1.00	0.90	77	1.04
70	2.8	25	1895	471	117.8	130.7	116.4	300	84.2	10.95	0.87	0.18	0.12	1.00	0.82	75	1.12
70	2.8	25	1895	471	117.8	130.7	116.4	500	84.2	10.95	0.87	0.18	0.12	1.00	0.82	75	1.12
70	2.8	25	1895	471	117.8	130.7	116.4	700	84.2	10.95	0.87	0.18	0.12	1.00	0.82	75	1.12
70	2.8	25	1425	834	208.4	131.9	123.8	150	102	6.14	0.65	0.16	0.24	0.95	0.95	93	1.10
70	2.8	25	1425	834	208.4	131.9	123.8	300	104	6.14	0.65	0.16	0.24	0.95	0.74	88	1.19
70	2.8	25	1425	834	208.4	131.9	123.8	500	104	6.14	0.65	0.16	0.24	0.95	0.70	86	1.21
70	2.8	25	1425	834	208.4	131.9	123.8	700	104	6.14	0.65	0.16	0.24	0.95	0.70	86	1.21
70	2.8	25	950	1875	468.9	135.2	131.5	150	115	2.75	0.48	0.15	0.35	0.88	0.99	111	1.04
70	2.8	25	950	1875	468.9	135.2	131.5	300	119	2.75	0.48	0.15	0.35	0.88	0.70	108	1.10
70	2.8	25	950	1875	468.9	135.2	131.5	500	119	2.75	0.48	0.15	0.35	0.88	0.57	108	1.10
70	2.8	25	950	1875	468.9	135.2	131.5	700	119	2.75	0.48	0.15	0.35	0.88	0.53	108	1.10
70	2.8	25	475	7502	1875.5	153.2	152.1	150	127	0.77	0.40	0.14	0.41	0.83	1.00	126	1.00
70	2.8	25	475	7502	1875.5	153.2	152.1	300	144	0.77	0.40	0.14	0.41	0.83	0.71	139	1.04
70	2.8	25	475	7502	1875.5	153.2	152.1	500	148	0.77	0.40	0.14	0.41	0.83	0.55	144	1.03
70	2.8	25	475	7502	1875.5	153.2	152.1	700	150	0.77	0.40	0.14	0.41	0.83	0.47	148	1.01
70	1.75	40	3045	183	45.6	50.7	45.1	150	29.8	10.97	0.87	0.18	0.12	1.00	0.82	29	1.02
70	1.75	40	3045	183	45.6	50.7	45.1	300	29.8	10.97	0.87	0.18	0.12	1.00	0.82	29	1.02
70	1.75	40	3045	183	45.6	50.7	45.1	500	29.8	10.97	0.87	0.18	0.12	1.00	0.82	29	1.02
70	1.75	40	3045	183	45.6	50.7	45.1	700	29.8	10.97	0.87	0.18	0.12	1.00	0.82	29	1.02
70	1.75	40	2293.5	322	80.4	50.9	47.8	150	37.8	6.14	0.65	0.16	0.24	0.95	0.71	33	1.13
70	1.75	40	2293.5	322	80.4	50.9	47.8	300	37.8	6.14	0.65	0.16	0.24	0.95	0.70	33	1.14
70	1.75	40	2293.5	322	80.4	50.9	47.8	500	37.8	6.14	0.65	0.16	0.24	0.95	0.70	33	1.14
70	1.75	40	2293.5	322	80.4	50.9	47.8	700	37.8	6.14	0.65	0.16	0.24	0.95	0.70	33	1.14
70	1.75	40	1529	724	181.0	51.4	50.0	150	44.1	2.71	0.48	0.15	0.35	0.88	0.62	41	1.07
70	1.75	40	1529	724	181.0	51.4	50.0	300	44.1	2.71	0.48	0.15	0.35	0.88	0.51	41	1.07
70	1.75	40	1529	724	181.0	51.4	50.0	500	44.1	2.71	0.48	0.15	0.35	0.88	0.50	41	1.07
70	1.75	40	1529	724	181.0	51.4	50.0	700	44.1	2.71	0.48	0.15	0.35	0.88	0.50	41	1.07
70	1.75	40	764.5	2896	724.0	54.1	53.7	150	51.6	0.70	0.40	0.14	0.41	0.82	0.59	50	1.03
70	1.75	40	764.5	2896	724.0	54.1	53.7	300	53.7	0.70	0.40	0.14	0.41	0.82	0.43	54	1.00
70	1.75	40	764.5	2896	724.0	54.1	53.7	500	55.6	0.70	0.40	0.14	0.41	0.82	0.35	56	0.99
70	1.75	40	764.5	2896	724.0	54.1	53.7	700	56.2	0.70	0.40	0.14	0.41	0.82	0.32	58	0.97
70	1.2	58.33	4455	85	21.3	23.8	21.2	150	12.6	11.02	0.87	0.18	0.12	1.00	0.82	14	0.92
70	1.2	58.33	4455	85	21.3	23.8	21.2	300	12.6	11.02	0.87	0.18	0.12	1.00	0.82	14	0.92
70	1.2	58.33	4455	85	21.3	23.8	21.2	500	12.6	11.02	0.87	0.18	0.12	1.00	0.82	14	0.92
70	1.2	58.33	4455	85	21.3	23.8	21.2	700	12.6	11.02	0.87	0.18	0.12	1.00	0.82	14	0.92
70	1.2	58.33	3345	151	37.8	23.8	22.4	150	16.3	6.11	0.65	0.16	0.24	0.95	0.70	16	1.04
70	1.2	58.33	3345	151	37.8	23.8	22.4	300	16.3	6.11	0.65	0.16	0.24	0.95	0.70	16	1.04
70	1.2	58.33	3345	151	37.8	23.8	22.4	500	16.3	6.11	0.65	0.16	0.24	0.95	0.70	16	1.04
70	1.2	58.33	3345	151	37.8	23.8	22.4	700	16.3	6.11	0.65	0.16	0.24	0.95	0.70	16	1.04
70	1.2	58.33	2230	340	85.1	23.9	23.3	150	19.6	2.68	0.48	0.15	0.35	0.88	0.50	19	1.02
70	1.2	58.33	2230	340	85.1	23.9	23.3	300	19.6	2.68	0.48	0.15	0.35	0.88	0.49	19	1.02
70	1.2	58.33	2230	340	85.1	23.9	23.3	500	19.6	2.68	0.48	0.15	0.35	0.88	0.49	19	1.02
70	1.2	58.33	1115	1361	340.4	24.5	24.4	150	24.2	0.68	0.40	0.14	0.42	0.82	0.41	25	0.98
70	1.2	58.33	2230	340	85.1	23.9	23.3	700	19.6	2.68	0.48	0.15	0.35	0.88	0.49	19	1.02
70	1.2	58.33	1115	1361	340.4	24.5	24.4	300	25.3	0.68	0.40	0.14	0.42	0.82	0.32	26	0.96
70	1.2	58.33	1115	1361	340.4	24.5	24.4	500	25.4	0.68	0.40	0.14	0.42	0.82	0.28	27	0.93
70	1.2	58.33	1115	1361	340.4	24.5	24.4	700	25.4	0.68	0.40	0.14	0.42	0.82	0.27	28	0.91
90	3.6	25	2440	470	117.5	130.7	116.4	150	80.4	10.99	0.87	0.18	0.12	1.00	0.90	77	1.04
90	3.6	25	2440	470	117.5	130.7	116.4	300	84	10.99	0.87	0.18	0.12	1.00	0.82	75	1.12
90	3.6	25	2440	470	117.5	130.7	116.4	500	84	10.99	0.87	0.18	0.12	1.00	0.82	75	1.12
90	3.6	25	2440	470	117.5	130.7	116.4	700	84	10.99	0.87	0.18	0.12	1.00	0.82	75	1.12

				Buckling analysis						Proposed DSM Design Approach							
b	t	b/t	L	f_{crft}	f_{cre}	f_{crf}	f_{crt}	f_y	f_u	Δ_f	a	b	c	d	β	f_{nfte}	f_u/f_{nfte}
90	3.6	25	1836	830	207.5	131.9	123.8	150	102	6.17	0.65	0.16	0.24	0.95	0.95	93	1.10
90	3.6	25	1836	830	207.5	131.9	123.8	300	104	6.17	0.65	0.16	0.24	0.95	0.74	87	1.19
90	3.6	25	1836	830	207.5	131.9	123.8	500	104	6.17	0.65	0.16	0.24	0.95	0.70	86	1.21
90	3.6	25	1836	830	207.5	131.9	123.8	700	104	6.17	0.65	0.16	0.24	0.95	0.70	86	1.21
90	3.6	25	1224	1868	466.9	135.2	131.5	150	115	2.76	0.48	0.15	0.35	0.88	0.99	111	1.04
90	3.6	25	1224	1868	466.9	135.2	131.5	300	119	2.76	0.48	0.15	0.35	0.88	0.70	108	1.10
90	3.6	25	1224	1868	466.9	135.2	131.5	500	119	2.76	0.48	0.15	0.35	0.88	0.57	108	1.10
90	3.6	25	1224	1868	466.9	135.2	131.5	700	119	2.76	0.48	0.15	0.35	0.88	0.53	108	1.10
90	3.6	25	612	7471	1867.6	153.1	152.0	150	127	0.77	0.40	0.14	0.41	0.83	1.00	126	1.00
90	3.6	25	612	7471	1867.6	153.1	152.0	300	144	0.77	0.40	0.14	0.41	0.83	0.71	139	1.04
90	3.6	25	612	7471	1867.6	153.1	152.0	500	148	0.77	0.40	0.14	0.41	0.83	0.55	144	1.03
90	3.6	25	612	7471	1867.6	153.1	152.0	700	150	0.77	0.40	0.14	0.41	0.83	0.47	148	1.01
90	2.25	40	3920	182	45.5	50.7	45.1	150	29.7	11.00	0.87	0.18	0.12	1.00	0.82	29	1.02
90	2.25	40	3920	182	45.5	50.7	45.1	300	29.7	11.00	0.87	0.18	0.12	1.00	0.82	29	1.02
90	2.25	40	3920	182	45.5	50.7	45.1	500	29.7	11.00	0.87	0.18	0.12	1.00	0.82	29	1.02
90	2.25	40	3920	182	45.5	50.7	45.1	700	29.7	11.00	0.87	0.18	0.12	1.00	0.82	29	1.02
90	2.25	40	2947.5	322	80.5	50.9	47.8	150	37.8	6.13	0.65	0.16	0.24	0.95	0.71	33	1.13
90	2.25	40	2947.5	322	80.5	50.9	47.8	300	37.8	6.13	0.65	0.16	0.24	0.95	0.70	33	1.13
90	2.25	40	2947.5	322	80.5	50.9	47.8	500	37.8	6.13	0.65	0.16	0.24	0.95	0.70	33	1.13
90	2.25	40	2947.5	322	80.5	50.9	47.8	700	37.8	6.13	0.65	0.16	0.24	0.95	0.70	33	1.13
90	2.25	40	1965	725	181.2	51.4	50.0	150	44.1	2.70	0.48	0.15	0.35	0.88	0.62	41	1.07
90	2.25	40	1965	725	181.2	51.4	50.0	300	44.1	2.70	0.48	0.15	0.35	0.88	0.51	41	1.07
90	2.25	40	1965	725	181.2	51.4	50.0	500	44.1	2.70	0.48	0.15	0.35	0.88	0.50	41	1.07
90	2.25	40	1965	725	181.2	51.4	50.0	700	44.1	2.70	0.48	0.15	0.35	0.88	0.50	41	1.07
90	2.25	40	982.5	2899	724.6	54.1	53.7	150	51.6	0.70	0.40	0.14	0.42	0.82	0.59	50	1.03
90	2.25	40	982.5	2899	724.6	54.1	53.7	300	53.7	0.70	0.40	0.14	0.42	0.82	0.43	54	1.00
90	2.25	40	982.5	2899	724.6	54.1	53.7	500	55.6	0.70	0.40	0.14	0.42	0.82	0.35	56	0.99
90	2.25	40	982.5	2899	724.6	54.1	53.7	700	56.3	0.70	0.40	0.14	0.42	0.82	0.32	58	0.97
90	1.54	58.33	5735	85	21.3	23.8	21.2	150	12.6	11.04	0.87	0.18	0.12	1.00	0.83	14	0.92
90	1.54	58.33	5735	85	21.3	23.8	21.2	300	12.6	11.04	0.87	0.18	0.12	1.00	0.83	14	0.92
90	1.54	58.33	5735	85	21.3	23.8	21.2	500	12.6	11.04	0.87	0.18	0.12	1.00	0.83	14	0.92
90	1.54	58.33	5735	85	21.3	23.8	21.2	700	12.6	11.04	0.87	0.18	0.12	1.00	0.83	14	0.92
90	1.54	58.33	4305	151	37.7	23.8	22.4	150	16.3	6.12	0.65	0.16	0.24	0.95	0.70	16	1.04
90	1.54	58.33	4305	151	37.7	23.8	22.4	300	16.3	6.12	0.65	0.16	0.24	0.95	0.70	16	1.04
90	1.54	58.33	4305	151	37.7	23.8	22.4	500	16.3	6.12	0.65	0.16	0.24	0.95	0.70	16	1.04
90	1.54	58.33	4305	151	37.7	23.8	22.4	700	16.3	6.12	0.65	0.16	0.24	0.95	0.70	16	1.04
90	1.54	58.33	2870	340	84.9	23.9	23.3	150	19.6	2.69	0.48	0.15	0.35	0.88	0.50	19	1.02
90	1.54	58.33	2870	340	84.9	23.9	23.3	300	19.6	2.69	0.48	0.15	0.35	0.88	0.49	19	1.02
90	1.54	58.33	2870	340	84.9	23.9	23.3	500	19.6	2.69	0.48	0.15	0.35	0.88	0.49	19	1.02
90	1.54	58.33	2870	340	84.9	23.9	23.3	700	19.6	2.69	0.48	0.15	0.35	0.88	0.49	19	1.02
90	1.54	58.33	1435	1359	339.7	24.5	24.4	150	24.2	0.68	0.40	0.14	0.42	0.82	0.41	25	0.98
90	1.54	58.33	1435	1359	339.7	24.5	24.4	300	25.3	0.68	0.40	0.14	0.42	0.82	0.32	26	0.96
90	1.54	58.33	1435	1359	339.7	24.5	24.4	500	25.4	0.68	0.40	0.14	0.42	0.82	0.28	27	0.93
90	1.54	58.33	1435	1359	339.7	24.5	24.4	700	25.4	0.68	0.40	0.14	0.42	0.82	0.27	28	0.91
															Mean		1.06
															Sd. Dev.		0.08
															Max		1.26
															Min		0.91